AD NUMBER

AD423236

NEW LIMITATION CHANGE

TO

Approved for public release, distribution unlimited

FROM

Distribution authorized to U.S. Gov't. agencies and their contractors; Administrative/Operational use; 19 Apr 1963. Other requests shall be referred to Defense Atomic Support Agency, Washington DC.

AUTHORITY

DNA ltr, 28 Jun 1973

NOTICE: When government or other drawings, specifications or other data are used for any purpose other than in connection with a definitely related government procurement operation, the U. S. Government thereby incurs no responsibility, nor any obligation whatsoever; and the fact that the Government may have formulated, furnished, or in any way supplied the said drawings, specifications, or other data is not to be regarded by implication or otherwise as in any manner licensing the holder or any other person or corporation, or conveying any rights or permission to manufacture, use or sell any patented invention that may in any way be related thereto.

[redacted] Y

POR-1803
(WT-1803)

Operation

NOUGAT

SHOT HARD HAT

PROJECT OFFICERS REPORT—PROJECT 3.3

FREE-FIELD GROUND MOTION STUDIES IN GRANITE (U)

William R. Perret

Sandia Corporation
Albuquerque, New Mexico

Issuance Date: April 19, 1963

[redacted]

Inquiries relative to this report may be made to

Chief, Defense Atomic Support Agency
Washington 25, D. C.

When no longer required, this document may be destroyed in accordance with applicable security regulations.

DO NOT RETURN THIS DOCUMENT

USAEC Division of Technical Information Extension, Oak Ridge, Tennessee

10 February 1964

ERRATA SHEET FOR POR-1803

FREE-FIELD GROUND MOTION STUDIES IN GRANITE (U)
(OPERATION NOUGAT, SHOT HARD HAT FINAL REPORT, PROJECT 3.3)

Page 6, Line 4: CHANGE: "784" to "730"
Line 6: CHANGE: "700" to "730"
Line 7: AFTER ". . . second zone)." INSERT: "Velocities are in feet per second and ranges in feet."

Page 17, Line 6: CHANGE: "was" to "were"

Page 18, Line 16: DELETE: "from the tunnel wall and floor."

Page 24, Last Line: DELETE: comma between "concerned" and "with."

Page 65, Line 18: CHANGE: "5.9g" to "4.5g"

Page 66, Line 1: CHANGE: "2.92-power" to "2.67-power"
Line 5: DELETE: Equation 5.2 and SUBSTITUTE:
"$a = 1.43 \times 10^{9} R^{-2.67 \pm 0.23}$" (5.2)

Page 67, Line 14: INSERT commas before and after "u".
Line 15: CHANGE: "1.10-power" to "1.23-power"
Line 19: DELETE: Equation 5.4 and SUBSTITUTE:
"$u = 2.24 \times 10^{4} R^{-1.23 \pm 0.40}$" (5.4)

Page 83: Figure 5.3 is superseded by the attached acceleration versus radial range graph.

Page 84: Figure 5.4 is superseded by the attached particle velocity versus radial range graph.

Page 96, Line 10: CHANGE: "2.92-power" to "2.67-power"
Line 12: CHANGE: "12.6 per cent" to "21 per cent"
Line 14: CHANGE: "$a = 7.18 \times 10^{9} R^{-2.92 \pm 0.27}$"
TO: "$a = 1.43 \times 10^{9} R^{-2.67 \pm 0.23}$"

Page 97, Line 4: CHANGE: "1.10-power" to "1.23-power"
Line 5: CHANGE: "22 percent" to "33 percent"
Line 6: CHANGE: "17.6 percent" to "31 percent"
Line 8: CHANGE: "$u = 9.26 \times 10^{3} R^{-1.10 \pm 0.24}$"
TO: "$u = 2.24 \times 10^{4} R^{-1.23 \pm 0.40}$"

Corrections for pages 65 through 97 are the result of revision of preliminary Stanford Research Institute data used to determine the second branch of acceleration and particle velocity attenuation curves. The new data are those included in the final SRI project report VUF-2101.

Military Distribution Category 14
USAEC Division of Technical Information Extension,
P. O. Box 401, Oak Ridge, Tennessee

POR-1803
(WT-1803)

OPERATION NOUGAT

SHOT HARD HAT

PROJECT OFFICERS REPORT – PROJECT 3.3

FREE-FIELD GROUND MOTION STUDIES IN GRANITE (U)

William R. Perret

Sandia Corporation
Albuquerque, New Mexico

ABSTRACT

Ground motion was observed by Project 3.3 at six stations between 256- and 784-foot range along a horizontal radius from the Hard Hat nuclear explosion in granite. Primary instrumentation comprised accelerometers oriented to respond to radial motion. Velocity and displacement gages backed up the accelerometers at five stations. At the two most remote stations, accelerometers and velocity gages were installed to respond to three orthogonal components of motion, radial, vertical, and tangential, the latter two directions being transverse to wave propagation.

Records were obtained from all gages, but early mechanical failure of some cables at very close-in stations limited the usefulness of those data. Results of analysis indicate that peak acceleration, a in g-units, is attenuated according to the equations

$$a = 9.89 \times 10^{15} R^{-5.12 \pm 0.26}$$

between 256- and 604-foot radial range, R in feet, and

$$a = 7.18 \times 10^{9} R^{-2.92 \pm 0.27}$$

between 604 and 1500 feet (based on inclusion of data from one Project 1.2 station).

Particle velocity u, in feet per second, is attenuated in accordance with the equations

$$u = 5.52 \times 10^{7} R^{-2.41 \pm 0.23}$$

between 306- and 784-foot range, and

$$u = 9.26 \times 10^{3} R^{-1.10 \pm 0.24}$$

between 700 and 1500 feet (again using Project 1.2 data to extend coverage in the second zone). Analysis of velocities shows onset of linear response of granite at about 730 feet and 4800 psi.

Displacement data indicate attenuation according to

$$\delta = 1.17 \times 10^{5} R^{-1.66 \pm 0.38}$$

where displacement δ is in inches.
Residual displacements are not very reliable, but suggest values of about 90 percent of peak displacement at 306-foot range, diminishing to about 20 percent at 604-foot range.

Stress and strain gages included at four stations gave data which were not wholly consistent, but which, at some stations, compared reasonably with values computed from particle velocities. Stress-strain ratios compared well with laboratory determinations of Young's modulus.

Strain measurements within the granite surrounding the access tunnel at two points, Stations 5+30 and 4+30, were undertaken for Project 3.1, and data from these measurements were delivered to that project for analysis.

CONTENTS

FIGURES*

*Numbers in parentheses are Sandia Corporation reference numbers for the figures.

TABLES

PREFACE

Field work, including all phases of instrumentation and data procurement, was accomplished by the Nuclear Test Department, 7250, of Sandia Laboratory. Joe W. Wistor was Project Leader in charge of this phase of the work. He was assisted by J. A. Beyeler, D. B. List, O. J. Birdsong, R. E. Foster, J. A. Kastning, E. S. Ames, H. E. Bell, H. E. Waldorf, and M. Triest.

All data reduction was done by the Test Services Division of Sandia Laboratory. Fred K. Millsap was directly responsible for converting all data from FM magnetic tapes to final digital and analog form.

Mr. Lawrence M. Swift of Stanford Research Institute has been a great help in bringing the final analysis of the Project 3.3 data to a more meaningful conclusion by furnishing unpublished data from Project 1.2 for that purpose.

Chapter 1

INTRODUCTION

1.1 BACKGROUND

The event which was carried out under the designation of Hard Hat had its origin as a part of the deep nuclear explosion experiment in granite planned as Project Lollipop of the Vela-Uniform program. Early in 1961, Project Hard Hat was activated to take over the original Lollipop location, U15a, as a detonation site.

Hard Hat, at one time, was under consideration alternatively as a nuclear or chemical explosives event, but resumption of underground nuclear testing in the fall of 1961 permitted final accomplishment of the original plan nearly intact.

1.2 OBJECTIVE

Hard Hat consisted of a 5.9-kiloton nuclear explosion at the bottom of a vertical boring about 960 feet beneath the surface of a granite stock in Area 15 of the Nevada Test Site. This project was incorporated in the Hard Hat program to define free-field motion and stress conditions on a horizontal radius in the immediate vicinity of the explosion.

Additional instrumentation on a vertical radius to the surface and at various ranges and azimuths over the surface, and at depth, were included, as was general seismological coverage to supply information to the Vela-Uniform program.

This report deals with Project 3.3, the particle motion study in granite on a horizontal radius from the detonation point, designed and executed by Sandia Laboratory to provide free-field information.

In addition to particle motion and stress measurements on the horizontal radius, strain measurements at several depths within the rock surrounding the access tunnel were made at ranges of 288 and 383 feet from zero.

The purpose of Project 3.3 was to define specifically free-field motion within the region of nonlinear response of granite to explosive loading from a multikiloton nuclear source. Instrumentation was to extend from as close to the source as feasible outward to include one or more stations beyond the range at which maximum stress falls below the elastic limit for granite.

Chapter 2

THE EXPERIMENT

2.1 ENVIRONMENT

Hard Hat shotpoint and tunnel are located within the Climax stock which is described (Reference 1) as an intrusive mass of igneous rock comprised of equigranular granodiorite and porphyritic quartz monzonite. Surface zero is within the outcrop areas of the stock.

Mineral content of the rock is roughly 28 percent (by volume) quartz, 22 to 35 percent potassium feldspar, 37 to 29 percent plagioclase, and 6.5 to 4 percent biotite. There are several major joint systems of which the most prominent dips from 15 to 35 degrees northeast, with an average strike of north 32 degrees west. These fractures are everywhere filled with chlorite, secondary feldspar, quartz, and sulfide minerals and tend to be structurally healed. Other principal joint systems dip at steeper angles, 45 to 85 degrees. These fractures are generally lined with clay minerals and are structurally weak. Frequency of the low-angle joints of the north 32 degrees west set varied between one and three per foot, while that of the steeper dipping sets was about one per foot.

Unconfined compression tests of cores from the quartz monzonite showed failure at between 8,000 and 9,000 psi, generally by tension fracture. Similar tests on granodiorite cores caused failure at loads ranging

from 6,700 to nearly 24,000 psi but averaging about 14,000 psi. Failure in the granodiorite was generally by tension, with a few shear failures.

Tests performed by Waterways Experiment Station (Reference 2) on cores from the vicinity of 845-foot depth yielded the following information.

Bulk density: 2.69 g/cc = 168 lb/ft^3

Tensile split strength: 1,915 psi

Compressive strength: 10,835 psi

Ultrasonic velocity (20 kc): 19,450 ft/sec

Modulus of elasticity, E: 11.3 x 10^6 psi

Poisson's ratio: 0.20

The Hard Hat tunnel intersected several fault and shear zones ranging in thickness from a few feet to nearly 30 feet and intersecting at angles ranging from nearly 90 to about 45 degrees.

2.2 DESIGN OF THE EXPERIMENT

The Hard Hat site in Area 15 included a shot hole, Station U15a, 36 inches in diameter and about 950 feet deep, and a 750-foot shaft giving access to a horizontal tunnel about 100 feet shallower than the burst point (see Figure 2.1).

The design of Project 3.3 instrumentation to fulfill its purpose of observing free-field motion and stress over a range extending from the region of hydrodynamic response into that of linear response, suggested that instruments should be located along a horizontal radius from zero. This ensured ease of gage orientation for true radial response and gage locations between 90 and 100 feet below the tunnel floor was free from perturbations which might be introduced by the free surface of the tunnel.

Instrumentation, as planned and installed for Project 3.3, is illustrated in Figure 2.1. This instrumentation was somewhat less than that planned for the corresponding Lollipop program, omitting only those stations which were to have been placed in borings not completed for the Lollipop effort.

Gage stations were located at the bottom of borings from the tunnel at six ranges distributed logarithmically between 250 and 800 feet. The radial component of motion was regarded as the primary measurement and was included at all stations. Additional particle-motion instrumentation was included at the two most distant stations to observe development of shear. Both vertical and horizontal tangential components of the motion were of interest here.

Reliability of accelerometers, established by broad field experience, made that type of gage the logical choice for primary instrumentation. However, development and successful use of SRI velocity gages for Scooter and Gnome measurements prompted their inclusion as backup instruments at all stations where predicted particle velocity fell within operational range for the gage.

Radial stress and strain in the free field within the region of expected nonlinear response of granite to the shock loading were of interest and were included at four stations between 300- and 600-foot range.

Plans for this project also included tests of two types of displacement gages under development at Sandia Laboratory. Both of these gages had been tested in the ground motion studies for Project Gnome.

Representatives of Project 3.1, Holmes and Narver and the University of Illinois, both of whom are concerned with response of the access tunnel, requested that measurements of strain be undertaken at several depths within the rock from the tunnel wall and floor at two stations along the tunnel. Subsequently, plans were made to include these measurements within Project 3.3, and strain gages were to be installed in NX borings at Section SS, slant range about 290 feet; and at Section TT, slant range about 385 feet (Figure 2.1). Original plans called for these gages to be installed at depths of 2, 4, and 8 feet within the rock from the mid-point of one wall of the tunnel, beneath and above the tunnel at the center of the floor and back, and on a 45-degree diagonal extending from the corner between wall and floor.

Limitations of information channels and feasibility of installation resulted in abandonment of borings above the tunnel and inclusion of the 2-foot-deep gages at the more remote station only. Strain-gage orientation was requested radial or normal to the tunnel axis and circumferential or parallel to the wall and normal to the axis.

2.3 SET-RANGE PREDICTIONS

Predictions of maximum motion for each gage station are necessary to permit proper choice of instruments and adjustment of recording equipment. The term set range refers to that magnitude of gage loading, usually somewhat greater than the predicted value, which analysis and judgment indicate will fall within the dynamic range of the gage and associated recording equipment, and which will ensure reliable interpretation of the signal in terms of gage calibration. Set range is always less than design range of the gage, generally by a factor of 2, but may be by a factor as great as 100.

Predictions for Hard Hat were those derived for Lollipop, altered shortly before installation to take advantage of data from similar measurements made during Project Gnome. The Lollipop predictions were based on Rainier experience, altered by scaling, and by a factor derived from the seismic impedances of tuff and granite. Accelerations, particle velocities, and displacements were obtained in this manner. Stresses and strains were derived from predicted velocities on the basis of elastic response relations. It was anticipated that strains, so predicted,

would be low by factors ranging to about 5, because of nonlinear effects, and set ranges were appropriately increased. Finally, preliminary data from the similar program of ground-motion observations included in Project Gnome became available before calibration of Hard Hat gages had begun. These data were especially pertinent to the Hard Hat program because of similarity of yields and rock characteristics for both events. Changes resulting from this feedback were generally an increase by a factor of about 2 above the original prediction, except for the closest accelerations, which were increased fivefold.

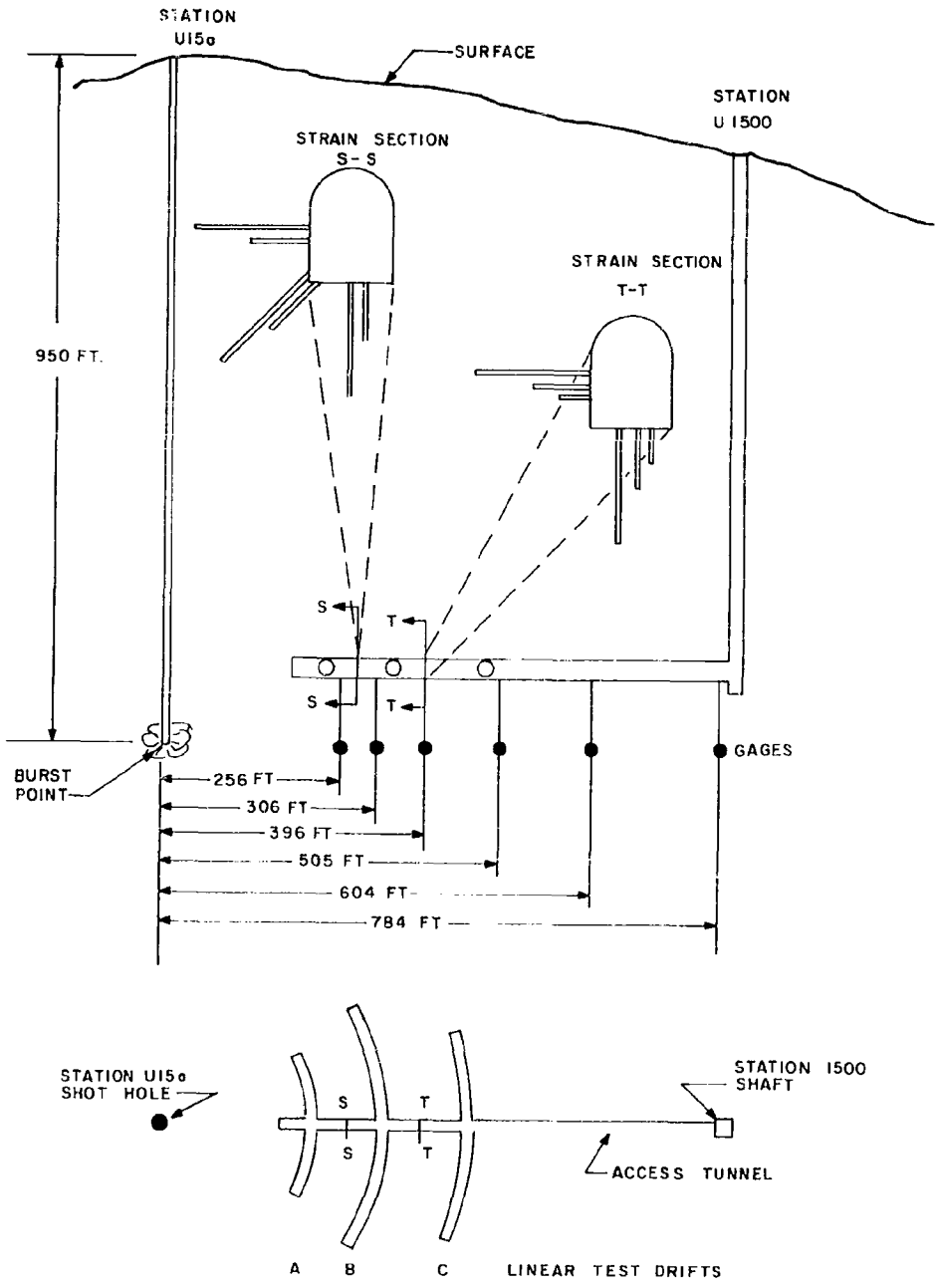

Figure 2.1 Site plan and elevation, Project 3.3 instrumentation.

Chapter 3

INSTRUMENTATION

3.1 INSTRUMENTS

All end instruments, accelerometers, velocity gages, displacement gages, and stress and strain gages used in Project 3.3 included either variable reluctance or differential transformer transducers. All gages were operated on 3-kc carrier-amplifier systems, Consolidated Engineering System D, through four conductor shielded cables. Output of the carrier-amplifier system was rectified and the resulting analog dc signal voltage was converted to a frequency-modulated signal which was recorded on magnetic tape. Six recorders, Ampex FR-114, were used at tape speeds of 60 inches per second. Center frequencies differed for different recorders, some were 54 kc and others 108 kc. Thirty-percent frequency deviation was used for set-range signal magnitude. The system responded linearly to 40-percent frequency deviation.

Accelerometers at the two shorter distances were Northam high-range instruments in which the active element is a diaphragm loaded by a small central mass (Figure 3.1). All other accelerometers were Wiancko instruments, in which an unbalanced mass is attached to one end of the armature adjacent to the E-coil transducer.

All velocity gages were of the overdamped pendulum type developed by Stanford Research Institute (Reference 3), Figure 3.2. These gages are basically grossly overdamped pendulums of relatively low natural frequency, about 5 cps, and are designed primarily to respond to horizontal motion. Under proper operating conditions they respond satisfactorily to velocity pulses such as damped sine or step functions. The two most critical limitations to proper operation of the gages are tilt sensitivity and degree of damping. It has been found that 0.5-degree tilt results in a transducer unbalance of about 25 percent of linear output range, and 2-degree tilt produces an unbalance of nearly full linear output. Damping equal to 100 times critical provides satisfactory velocity response.

These velocity gages may be modified to respond to vertical motion by installation of a spring (Figure 3.3) between the pendulum vane and case, to counteract gravity and support the pendulum in equilibrium position. Characteristics of the modified gage are in general similar to those of the original one, except that it appears to be less sensitive to tilt.

Displacement gages were of two types, a long-base strain gage mounted to respond to tangential strains (parallel to the wave front) and an inertial-mass-type gage. The first of these is a modification of the relative displacement gage used for Project 1.5 during the Priscilla event of Operation Plumbbob (Reference 4). These gages had a 10-foot base length and used a rigid rod supported at intervals by nylon bushings as the coupling element, rather than a spring-loaded wire. Schaevitz linear differential transformers were the transducer elements.

Inertial displacement gages have recently been developed by SRI and Sandia. These gages are similar in principle, in that travel of an inertial mass is measured and demagnification is accomplished by causing the inertial mass to drive a flywheel. The Sandia gage (Figure 3.4), which was proof-tested during the Gnome and Hard Hat events, was designed for observation of horizontal displacements. It consists of a mass riding on ball-bushings and a splined shaft. The flywheel is driven through a rack and pinion by motion of the mass along the shaft. A rotary differential transformer converts motion to an electrical signal. Provision is made for remote leveling of these gages because of their obvious sensitivity to tilt.

Stress and strain gages were similar, in that both used Schaevitz linear differential transformers to observe deformation of material under load. The strain gages comprised differential transformers mounted in granite cores (Figure 3.5). These cores were machined to pass into the nominal 8-inch-diameter vertical borings. Because these borings were not reamed to the required size, it was necessary to trim the cores to about 4-inch diameter. Strain gages for the NX borings, nominal 3-inch diameter, in Sections SS and TT were installed in blocks of granite (Figure 3.6). These blocks of 2-inch-square cross section were resorted to when no cores capable of entry into the NX borings were available and no facilities for turning down oversize cylindrical cores could be found. The change in shape was accepted by both parties concerned, with analysis of these data.

Stresses were measured with gages similar to those developed for Operation Hardtack II by Sandia Laboratory. These gages comprise right circular cylinders of aluminum or other material which are loaded axially through rigid steel plates and which accommodate, through an axial hole, Schaevitz linear differential transformers to measure axial deformation. They are calibrated under static load so that axial deformation is relatable to applied pressure. This assumes that the loads remain within the elastic limit of the strained material and that response under dynamic loads is wholly analogous to that under static loads. Figure 3.7 shows a stress gage mounted above a strain-gage core.

3.2 CALIBRATION

Calibration of all Project 3.3 gages was carried out in a building within the Sandia Compound near the NTS Control Point, rather than in Area 15, because of impracticality of calibration in the tunnel and problems of weather and existing facilities. All gages were calibrated on appropriate lengths of cable similar to that installed at the Hard Hat site. Accelerometers were calibrated on a spin table except where set ranges were 2 g or less. In the latter case, inversion of the gage in the earth's gravitational field permitted adequate calibration.

Velocity gages were calibrated by cocking the pendulum and observing the output as a function of time upon release. The gages were rotated so that the pendulum would fall through a horizontal position after release from the cocked position.

Strain gages and the long-span gage were calibrated by static displacement of the transformer core through proper set-range distances. Inertial displacement gages were calibrated by direct movement of the mass through measured distances which were fitted to a multiplier factor introduced by the flywheel and previously determined by analysis and verified on a calibration sled.

Both the long-span gage and inertial displacement gage included means for remote adjustment which also permitted a calibration check after they were grouted in place.

Each channel included a calibration signal device which introduced a voltage signal precisely related to set range for the gage. The calibration device was so installed in the recording circuit that its signal related gage signal directly to sense and magnitude of the driving motion or force. A cal signal was inserted in the circuit for 10 seconds at -30 seconds and again at about +3 minutes. Thus, there was a calibration check on the entire recording system immediately before and after the signal of interest.

3.3 INSTALLATION

All gages were calibrated, and assemblies for each boring were completed at the calibration building in the Sandia Compound. Cables for all instrument stations on the horizontal radius were spiraled on elastic shock cord and encased in a flexible armored tubing of sufficient length to extend about 50 feet along the tunnel beyond the boring collar. Completely

assembled instruments and cables for each station were transported as a unit (Figure 3.8). Instruments for the tunnel strain measurements were handled in a similar manner, except that cables from these gages were carried through the boring and into the tunnel in standard electrical conduit.

3.3.1 Installation of Horizontal-Radius Gages

Gage assemblies for each deep boring were transported to the site for installation, and gage cables were spliced to appropriate cables previously laid from the recording trailer to each boring station. Each gage was monitored after arrival at the station boring and at intervals during installation. An orienting rod was attached to the gage assembly, and proper alignment of gages toward the burst point was maintained throughout placement and initial grouting. Gage response axes were positioned within 5 degrees of assigned directions.

Grout hose was run into the borings after gages were in place, and a grout designed for approximate match to granite was pumped to a level about 4 feet above the uppermost gage. This grout was allowed to set for several hours before the orienting rod was withdrawn. Additional grout was pumped to completely fill the boring. This final step was not followed for Boring 6, but rather, dry-sand backfill was used above the first-stage grout to determine whether any advantage to cable survival resulted.

Design of the grout was accomplished by the Concrete Research Division of the U. S. Corps of Engineers Waterways Experiment Station as a part of Project 9.1. Specimens of the grout were taken during installation, and these were tested shortly after Hard Hat detonation. Results of these tests, compared with results of similar tests of granite cores previously quoted, were:

Parameter	Grout	Rock
Density	2.7	2.69
Ultrasonic velocity	12,000 ft/sec	19,450 ft/sec
Compressive strength	7,200 psi	10,835 psi

A small sample of grout recovered after re-entry from a shallow boring in the tunnel wall was found to have a density of about 2.55.

It should be noted that the deep borings which were to have been of nominal 9-inch-diameter were, in fact, full diameter to depths of only about 10 feet. Below that point, diameters were about 7 inches. This necessitated revision of strain-gage core diameters to 4 inches. Following this revision, all instrument assemblies could be placed at desired positions in the borings, with the exception of that for Boring 8, which jammed at a point about 9 feet above the assigned depth and was grouted at that position.

All gages were monitored following completion of grouting, and calibration of the inertial displacement and long-span gages was checked. Velocity-gage fall times were also checked by cocking and releasing the pendulums.

3.3.2 Installation of Tunnel Strain Gages

Strain gages for tunnel measurements were assembled and transported to the appropriate site; cable splices were made and gages monitored before installation. A small quantity of grout was placed at the base of each boring, and the gages were seated securely before grout was pumped in under pressure.

Cables for these gages were carried out of the borings in rigid metal conduit which was used for orienting the gages prior to grouting. Since these borings were all 8 feet or less in depth, use of conduit was feasible and was not considered to introduce significant perturbation.

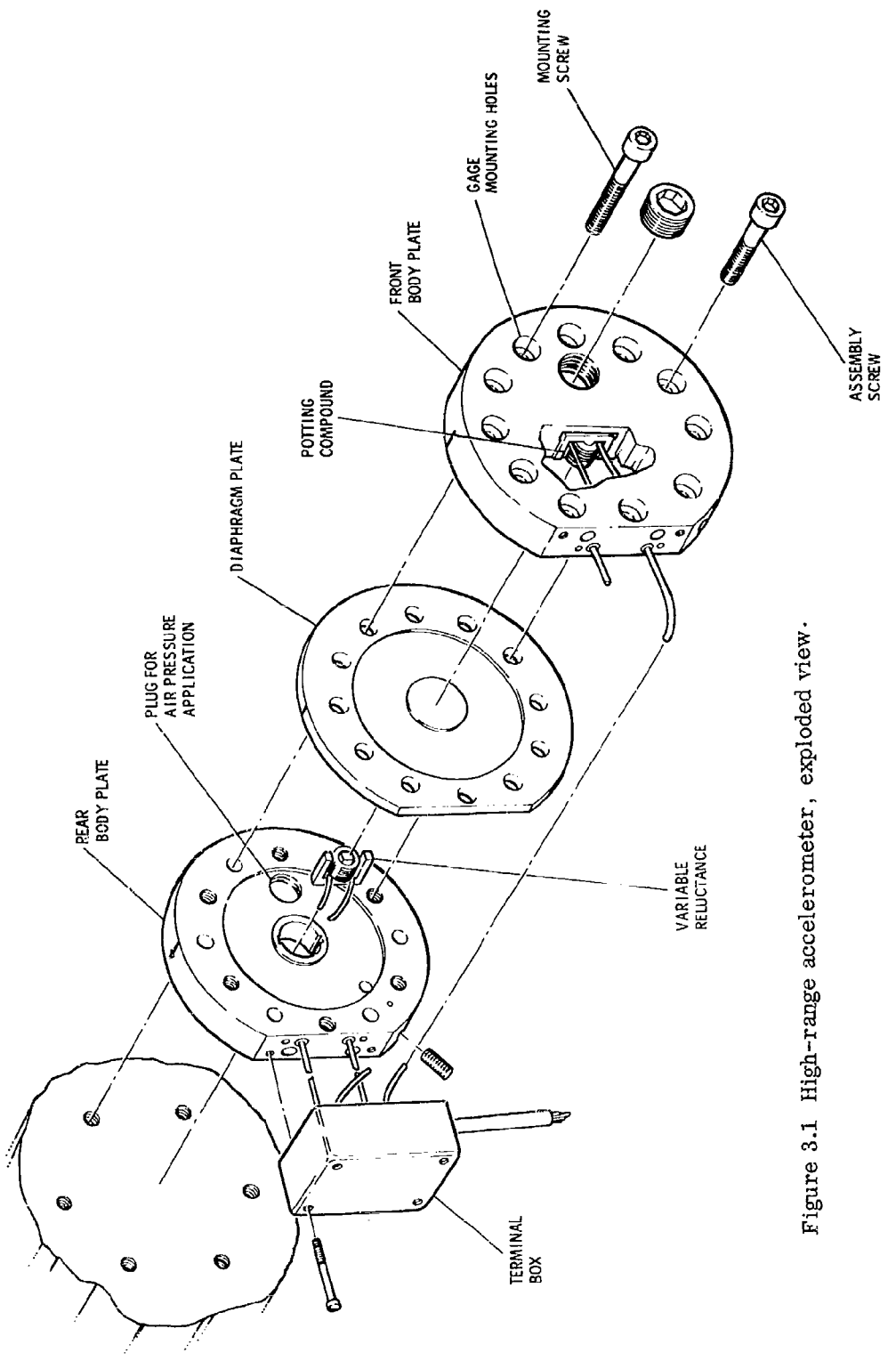

Figure 3.1 High-range accelerometer, exploded view.

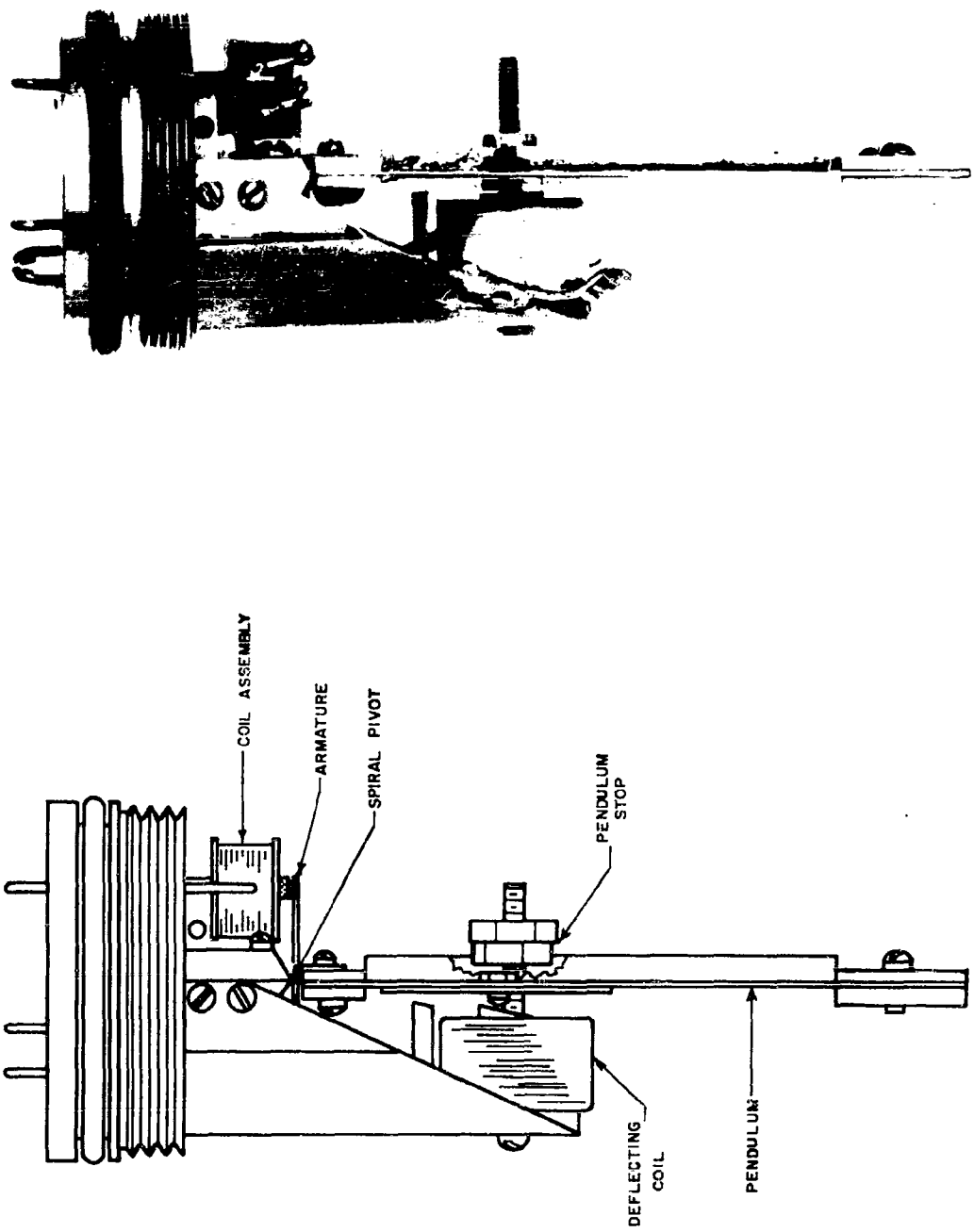

Figure 3.2 SRI horizontal velocity gage.

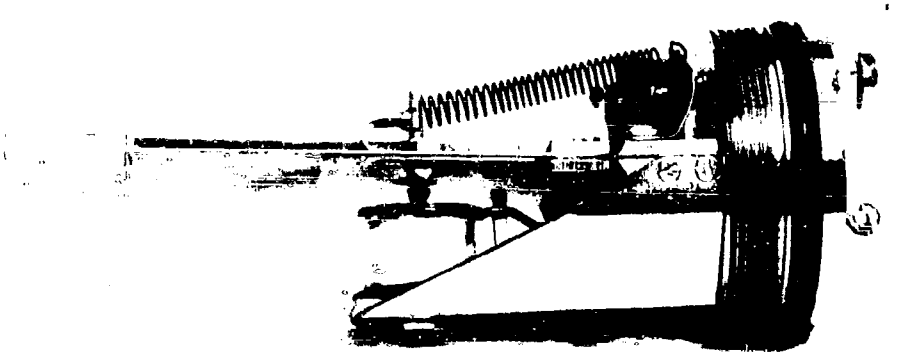

Figure 3.3 SRI velocity gage modified for vertical response.

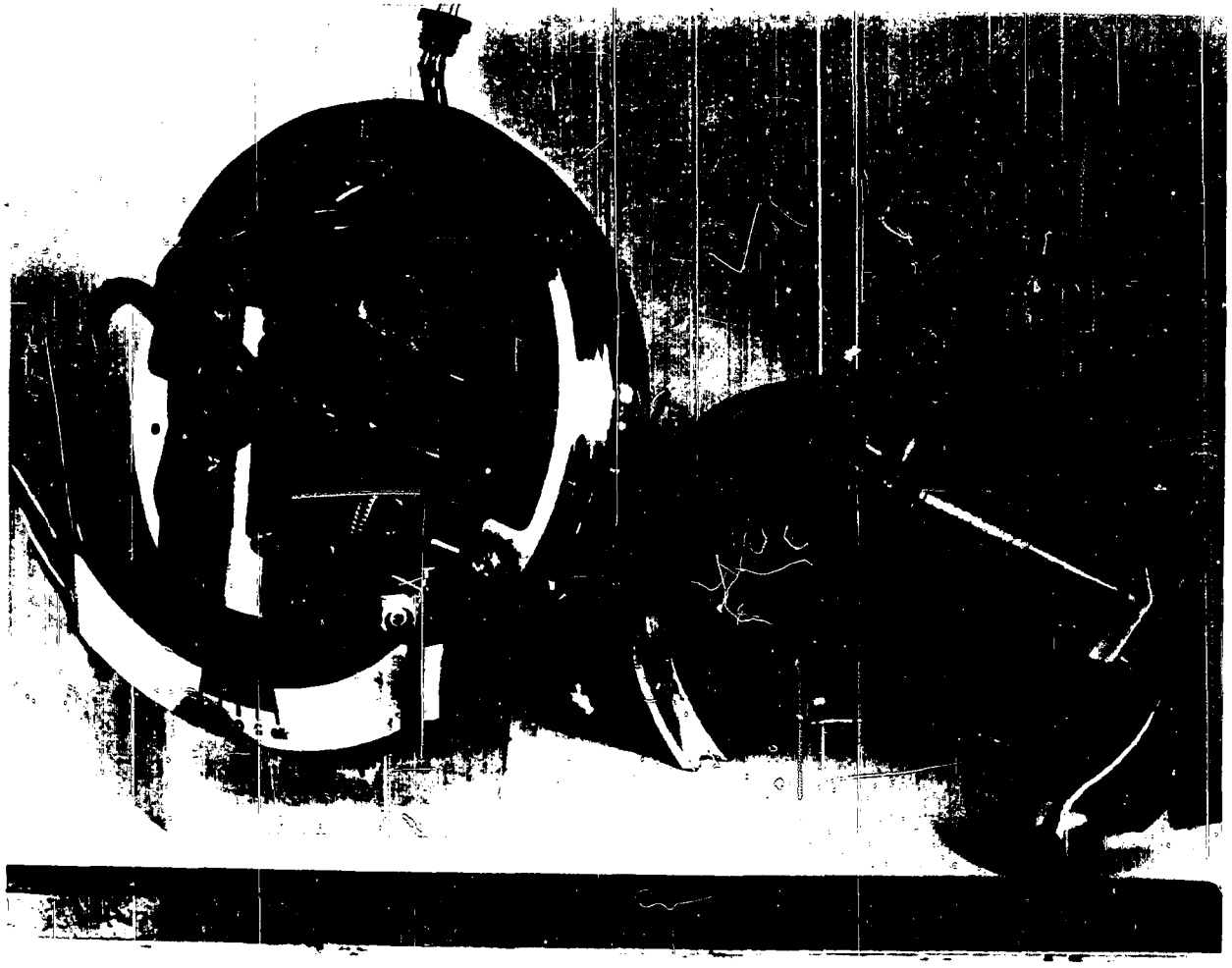

Figure 3.4 Sandia Laboratory inertial displacement gage.

Figure 3.5 Strain gage in granite core.

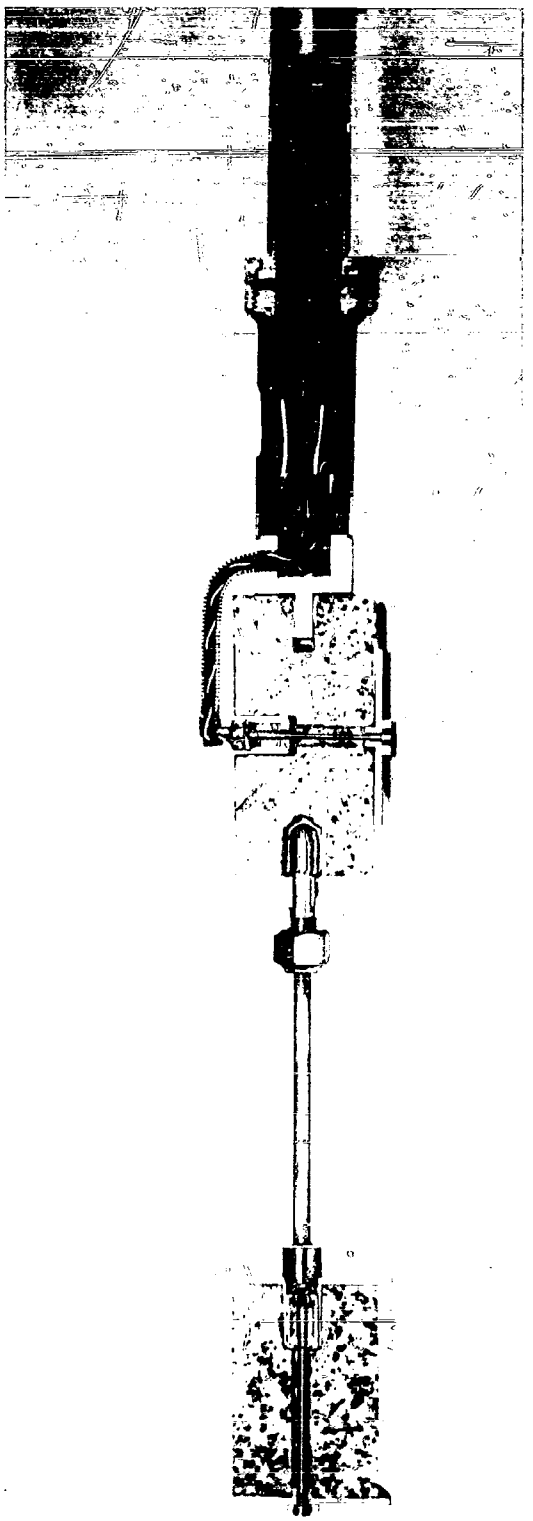

Figure 3.6 Strain gages for Tunnel Section SS.

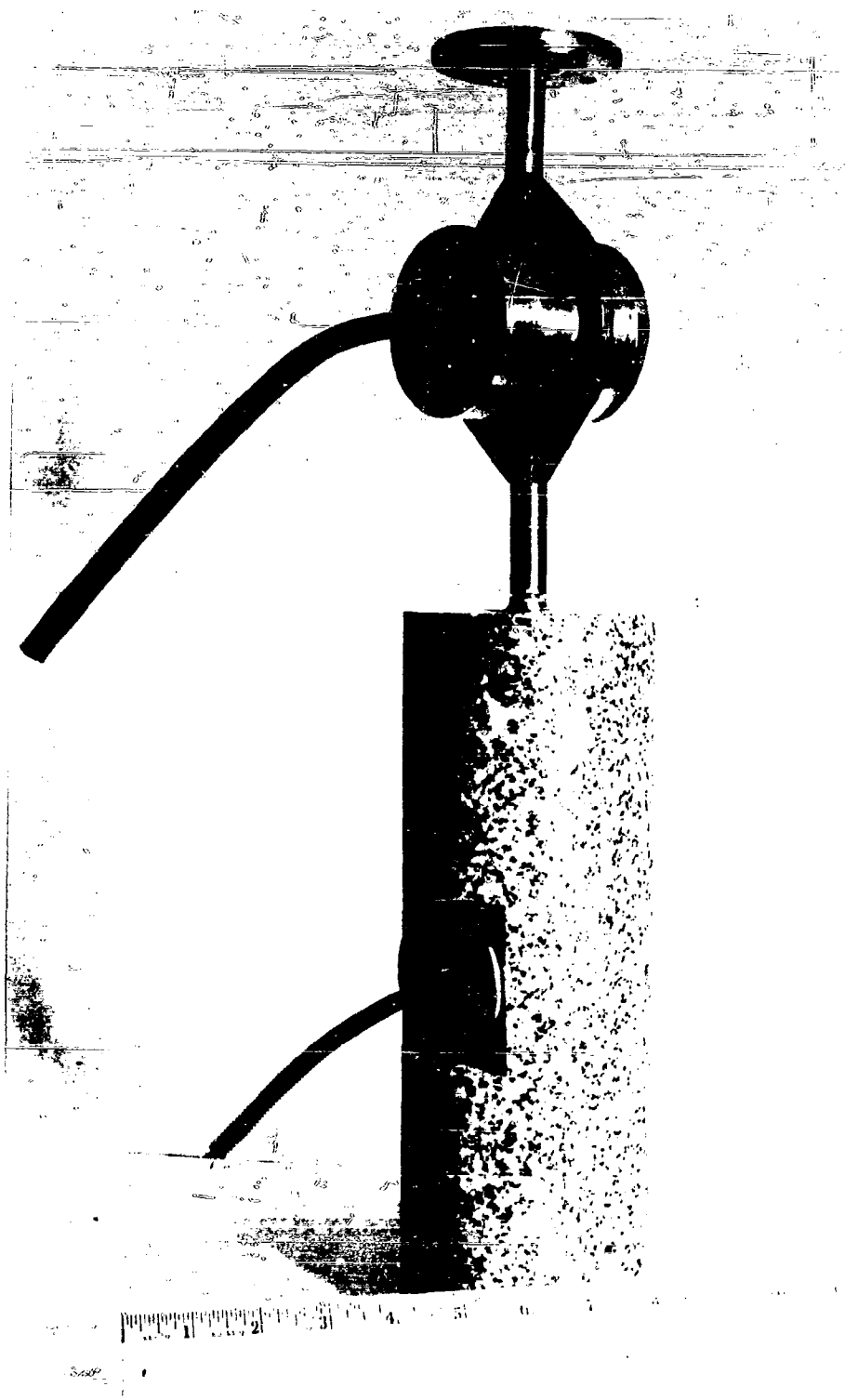

Figure 3.7 Stress and strain gage assembly.

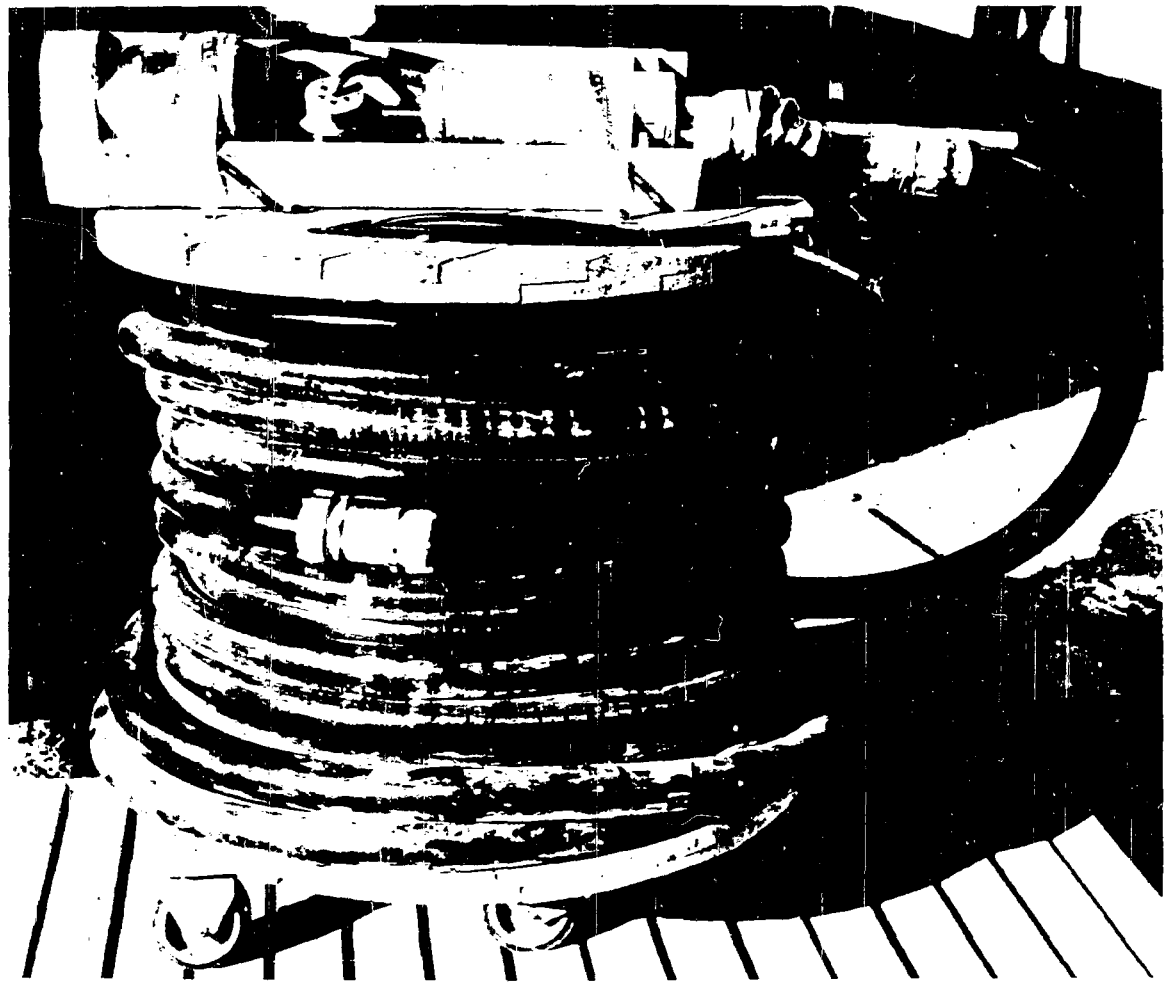

Figure 3.8 Gage and cable assembly prepared for installation, Boring 6.

Chapter 4

RESULTS

4.1 DATA ACQUIRED

There were 31 information channels installed in the horizontal-radius portion of Project 3.3 and 22 channels in the tunnel-strain sections. Of these 53 channels, preshot checks showed that two of those on the horizontal radius, the strain gage in Boring 8 and the vertical velocity gage in Boring 12, were inoperative and that high-resistance short circuits to ground in four of the tunnel strain channels might affect results adversely.

All recorders operated satisfactorily, and legible records were obtained from playback of 50 channels. Some of these were of short duration because of cable damage, but all included real signal and first peak motion.

4.2 DATA REDUCTION

Data recorded on the magnetic tapes were converted to digital and analog forms. Processing of data from each channel required three to five stages: (1) oscillographic playback from the tape to provide early rough data and to serve as a basis for scheduling sampling rate and time duration for digitizing; (2) digitization directly from the tape; (3) computer runs to introduce real time and calibration information and to perform initial

integration of acceleration and velocity data; (4) correction of velocity data, where applicable, to minimize effects of accelerometer zero changes or velocity gage tilt; and (5) corrected integrations and machine plots of all data. Of course, for all records except those from accelerometers and velocity gages, plotting follows the third step, since integration was not pertinent and corrections were not feasible.

Corrections applied to certain channels have been based upon two conditions: first, that particle velocities must vanish at some time after the first positive phase and at a time usually discernible from the velocity record; and second, that when a velocity gage is tilted, a shift in the equilibrium position and, therefore, in the record zero occurs. These corrections do not normally produce significant changes in peak values but do affect latter parts of the data radically. It should be noted also that these corrections as applied to original data are small, rarely exceeding one percent of accelerometer set range.

4.3 RECORDS

4.3.1 Records from Horizontal-Radius Gages

Plotted data from gages at each station on the horizontal radius from Hard Hat are presented in Figures 4.1 through 4.10. They are arranged to indicate variations of recorded data with increasing radial range and to compare recorded with derived data in the case of particle velocity and displacement. Gages on the horizontal radius are identified by a code which indicates the boring, motion parameter, and component. In this code,

numbers identify the boring; A indicates acceleration; U, velocity; D and DI, displacement (I indicates the inertial gage); F, stress; and L, strain. V refers to vertical component, R to radial, and T to tangential. Where no component is indicated, it is understood that gage response is radial. Thus, 6-A is the accelerometer in Boring 6 at 306 feet from the explosion at source level oriented to respond to radial motion, and 12-UV is the velocity gage in Boring 12 at 784 feet from the explosion at source level oriented to respond to vertical motion.

Information derived from these data and pertinent to project performance is assembled in Table 4.1. These data include gage locations and set ranges as well as arrival times and peak values.

Certain features of some records deserve discussion here. In particular, cables from gages in Borings 4, 6, and 9 were severely damaged at progressively later times, breaking between 19 and 22 milliseconds at Boring 4, between 43 and 55 milliseconds at Boring 6, and between 44 and 550 milliseconds at Boring 9. Cables from three gages in Boring 8, all but two gages in Boring 11, and all gages in Boring 12 were intact at the time of postshot checks during record recovery. Damaged cables from Borings 8 and 11 were intact through 500 milliseconds or longer after detonation.

Two gages failed to give records. One, 8-L, was a strain gage for which all electronics functioned satisfactorily, including the calibration. It is not presently clear what could have caused the malfunction in this channel, but no strain was recorded at Boring 8. The vertical velocity gage in Boring 12 gave no data because, after installation, it was found impossible to attain

a legitimate circuit balance. Again it is not clear what the source of difficulty was, but we suspect that the vane-supporting spring became disconnected so that the vane rested upon its lower stop.

The exact time at which the cable from accelerometer 4-A in Boring 4 was damaged is not certain from the record. The first recorded peak occurred at 18.9 milliseconds after detonation and was followed by a very steep drop to a negative acceleration nearly twice the first peak. It is possible that the first peak is not the true one; cable damage may have occurred prior to arrival of the true peak acceleration. There is no evidence that gage performance was affected, and correlation with records from more remote gages suggests that the observed peak is probably the true one.

Cable damage did not affect the initial peaks of any other records. And, with a few exceptions, cable damage did not seriously affect the positive-phase portions of velocity records either derived or directly recorded, with the exception of the integrated 4-A record.

The inertial displacement gage, 8-DI, appears to have undergone either extreme radial motion, or the gage-reaction equivalent, tilting,in a radial direction (Figure 4.11). These gages, as previously noted, are very sensitive to tilt parallel to the response axis. Relatively long-period rolling motion could cause the gage mass to travel to the stops at each end of the splined shaft alternately as suggested by the record from 8-DI. It is noteworthy that the gage range was established so that about twice as much travel was permitted outward (positive) as inward

for the radially oriented gage, and the recorded maxima are 24 inches outward and 13.5 inches inward with a set range of 13 inches. These are not to be interpreted as real displacements but as indeterminate angular tilts which persisted long enough to let the mass move against the stop.

Stress gages in Borings 6, 8, and 9 (Figure 4.9) recorded a stress wave of the general type expected, except that none indicated a real negative-phase pressure. However, both construction of the gage and the material used would act to prevent indication of a true negative pressure, i.e., less than ambient. Some residual strain is to be expected in the aluminum used in the gages response element, and the fact that there is evidence of a temporary drop to 500 psi before the apparent residual of about 900 psi is established suggests that a negative-phase pressure of about 400 psi occurred at Gage 8-F. Such negative pressure is probably not a true tension but rather a reduction of compressive stress, since geostatic pressure at the gage level is about 1100 psi.

The stress gage in Boring 11 reacted differently from those closer to Hard Hat source, in that indicated residual stress is about 80 percent of the peak value. This is probably attributable to the difference in gage-element material, nylon, used in 11-F in place of aluminum. Peak stress observed in Boring 11 is probably meaningful, but, beyond the peak, data are of doubtful value. Here again, there is a suggestion of a 250-psi negative-phase pressure.

Strain-gage records, except in Boring 11, suffered from cable damage before completion of positive phase and, in the case of 8-L, from an unknown malady which permitted no signal to be generated.

The signal-noise ratio is poor for both 6-L and 9-L because peak signals were only about 5 and 8 percent of gage set range. The situation is much better for 11-L, for which the signal was about 18 percent of set range.

Analogous comments might be made concerning signal-noise values for other gages, but it is considered that the foregoing discussion and tabulation of peak values and set ranges (Table 4.1) give a fair picture of over-all significance of differences in predictions and observations.

4.3.2 Records from Tunnel Cross Sections

Records from 19 of the 22 strain gages installed at Sections SS and TT were legible and indicate strain for periods ranging from about 20 milliseconds to as long as 1000 milliseconds, before cable damage affected the records.

Strain gages at these sections are identified by S or T for the section; N or C for normal (radial) or circumferential gage-response orientation; and either W for wall, D for diagonal, or B for floor, and a number indicating depth of the gage from the wall. Thus, SN-D8 refers to a gage at Section SS oriented to respond to strain normal to the tunnel axis along an extended tunnel radius. The gage is in a boring drilled from the corner between tunnel wall and floor at 45 degrees, sloping downward and situated 8 feet deep in rock from the tunnel surface.

Records from Section SS are presented in Figures 4.12 through 4.14. They are arranged to compare radial with circumferential strains at 4- and 8-foot depths from the wall, corner, and floor. Apparent time of cable damage is identified on each record.

All records from Section TT are presented in Figure 4.15. It should be noted that in this figure one record, TN-B8, is plotted for a considerably longer time than are the others. Peak strains and other pertinent information from both sections are assembled in Table 4.2.

These data were obtained for Project 3.1 and will not be analyzed for this report, but it is pertinent to note certain features of the records. At Section SS, at both 4- and 8-foot depths, maximum radial strains are tensile and are larger than circumferential strains, which are compressive. Gages below the floor at this location show large compressive strains in both radial and circumferential directions. At Section TT, all strain maxima were tensile with the exception of the circumferential strain at 8 feet beneath the tunnel floor.

One gage, TC-W2, was recovered after the shot because the wall had spalled sufficiently to make removal of the gage easy. Inspection showed that the granite block had apparently split parallel to the axis of the transformer, Figure 4.16. Such a break might be expected to relieve nearly all strain and may be interpreted as having caused the sudden drop in strain shown on the record from this gage at about 147 milliseconds. At the time of recovery, it was noted that the grout which held this gage in place was intact and was well bonded to both the granite block and the boring wall. A piece of the grout appears to the right of the granite in Figure 4.16.

The evidence just described for a break in the core as a source of strain relief may, by inference, account for similar sharp decreases in strain on all records from Section TT except the two at 8 feet beneath the tunnel floor.

Both of the latter gages showed no evidence of radical change in strain throughout the recording period of over 1 minute. It should be noted, however, that of all the strain gages at the two tunnel sections, only those 8 feet beneath the floor at Section TT were served by cables which were intact at the postshot check. All other cables were damaged and showed open circuits at the postshot check; hence, the conclusion, that the recorded drop in strain is strain relief, cannot be verified, and we must be content with speculation that it could be either a split core or a broken cable.

TABLE 4.1 DATA FROM HORIZONTAL RADIUS, PROJECT 3.3

Gage Number	Horizontal Range	Time of Arrival	Acceleration	Velocity	Displacement	Stress	Strain	Set Range
	ft	msec	g	ft/sec	in.	psi	%	
4-A	256	14.1	4226	56.5*	-	-	-	6,000
6-A	306	17.1	1946	60.6	6.4 (5.5)	-	-	1,500
6-U	306	18.5	-	51.3	1.4 (1.3)	-	-	150
6-F	306	17.0	-	-	-	14,036	-	30,000
6-L	306	17.1	-	-	-	-	0.15	3.0
8-A	396	22.0	493	30.1	8.5 (5.2)	-	-	700
8-U	396	23.1	-	30.0	7.1 (3.4)	-	-	60
8-DI	396	23.0	-	-	3.9	-	-	10
8-F	396	21.9	-	-	-	13,051	-	20,000
8-L	396	-	-	-	-	-	No data	0.3
9-A	505	28.0	215	21.4	5.6	-	-	200
9-U	505	28.8	-	8.0	2.5	-	-	50
9-DI	505	28.5	-	-	6.8	-	-	6
9-F	505	28.3	-	-	-	2,230	-	12,000
9-L	505	28.7	-	-	-	-	0.16	0.2
11-AR	604	33.0	46.0	6.0	1.8 (0.19)	-	-	100
11-AV	604	33.6	22.3	1.9	4.9	-	-	100
11-AT	604	33.0	57.2	10.2	1.4	-	-	100
11-UR	604	36.1	-	5.2	0.7	-	-	40
11-UV	604	35.2	-	2.2	4.4	-	-	40
11-UT	604	34.6	-	11.0	3.8	-	-	40
11-DI	604	35.0	-	-	6.7 (0.5)	-	-	6
11-F	604	33.5	-	-	-	4,423	-	10,000
11-L	604	33.3	-	-	-	-	0.037	0.1
12-AR	784	42.5	32.7	5.7	1.98	-	-	80
12-AV	784	42.5	12.4	1.5	0.13	-	-	80
12-AT	784	42.6	23.9	4.1	0.62	-	-	80
12-UR	784	43.7	-	7.4	2.6 (1.5)	-	-	20
12-UV	784	-	-	No data	-	-	-	20
12-UT	784	44.6	-	3.9	1.05	-	-	20
12-D	784	47.7	-	-	1.05 (0.2)	-	-	16

*Not a true peak.

Note: Displacements in parentheses are recorded residuals.

TABLE 4.2 STRAIN DATA FROM TUNNEL CROSS SECTIONS, PROJECT 3.3

Gage Number	Section	Depth	Time of Arrival	Strain	Sense	Direction	Cable Break	Set Range
		ft	msec	%			msec	%
SN-W4	SS*	4	15.7	2.1	Tens	Radial	22.0	1.3
SC-W4	SS	4	15.3	0.50	Compr	Circum	22.6	1.0
SN-W8	SS	8	18.0	0.20	Tens	Radial	21.5	1.3
SC-W8	SS	8	15.4	0.16	Compr	Circum	18.7	1.0
SN-D4	SS	4	15.2	2.1	Tens	Radial	21.6	1.3
SC-D4	SS	4	15.8	0.37	Compr	Circum	28.5	1.0
SN-D8	SS	8	15.8	0.99	Tens	Radial	23.7	1.3
SC-D8	SS	8	13.0	0.20	Compr	Circum	23.5	1.0
SN-B4	SS	4	15.3	0.26	Compr	Radial	22.8	1.3
SC-B4	SS	4	15.0	0.34	Compr	Circum	23.7	1.0
SN-B8	SS	8	15.4	0.14	Compr	Radial	19.0	1.3
SC-B8	SS	8	15.8	0.074	Compr	Circum	19.1	1.0
TC-W2	TT**	2	21.8	0.51	Tens	Circum	156	1.0
TN-W4	TT	4	23.0	2.0	Tens	Radial	158	1.3
TC-W4	TT	4	21.8	1.2	Tens	Circum	152	1.0
TN-W8	TT	8	27.0	0.90	Tens	Radial	174	1.3
TC-W8	TT	8	21.9	0.54	Tens	Circum	167	1.0
TC-B2	TT	2	-	No data	-	Circum	-	1.0
TN-B4	TT	4	21.8	0.05	Tens	Radial	35	1.3
TC-B4	TT	4	23.0	0.04	Compr	Circum	32	1.0
TN-B8	TT	8	24.9	1.4	Tens	Radial	-	1.3
TC-B8	TT	8	22.6	0.23	Compr	Circum	-	1.0

*Average slant range to Section SS is 288 feet.
**Average slant range to Section TT is 383 feet.

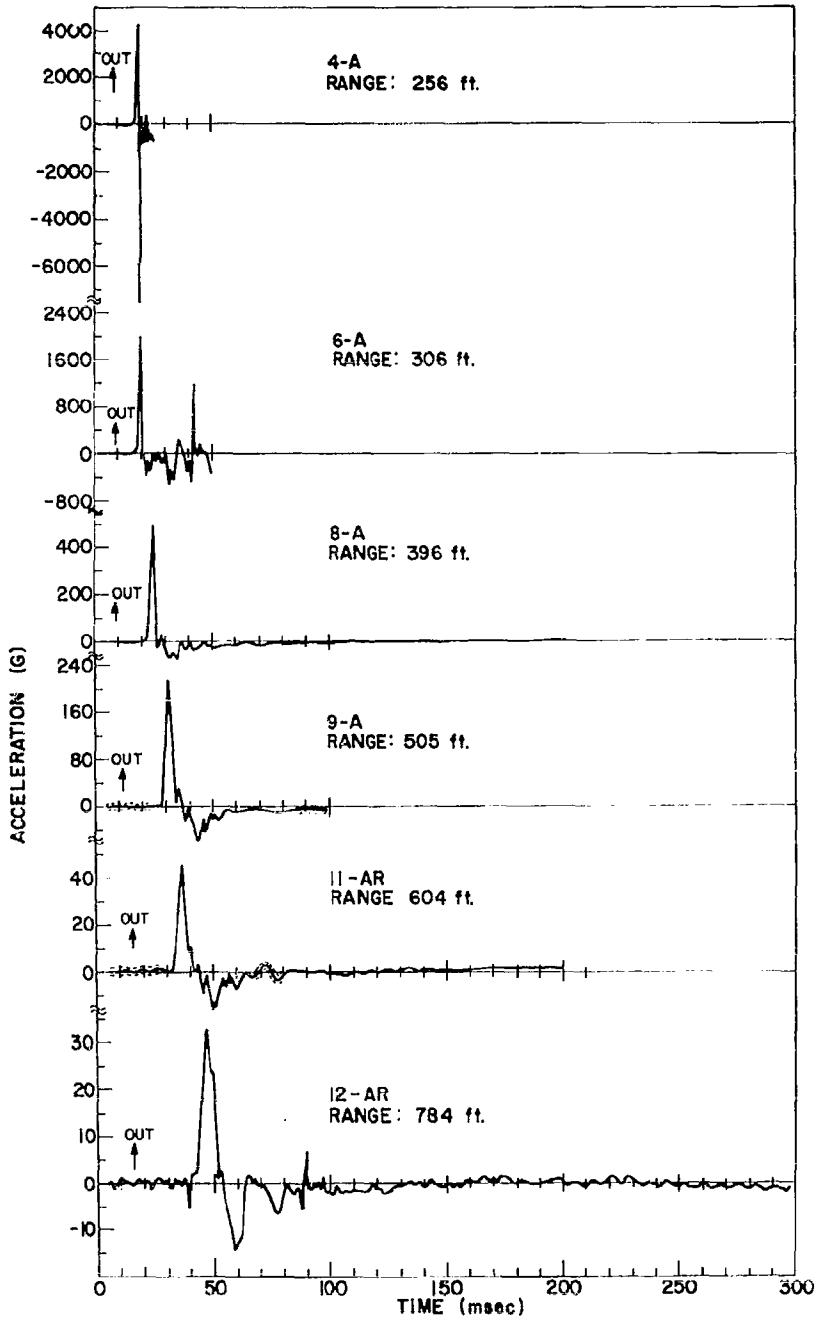

Figure 4.1 Radial accelerations, Borings 4 through 12.

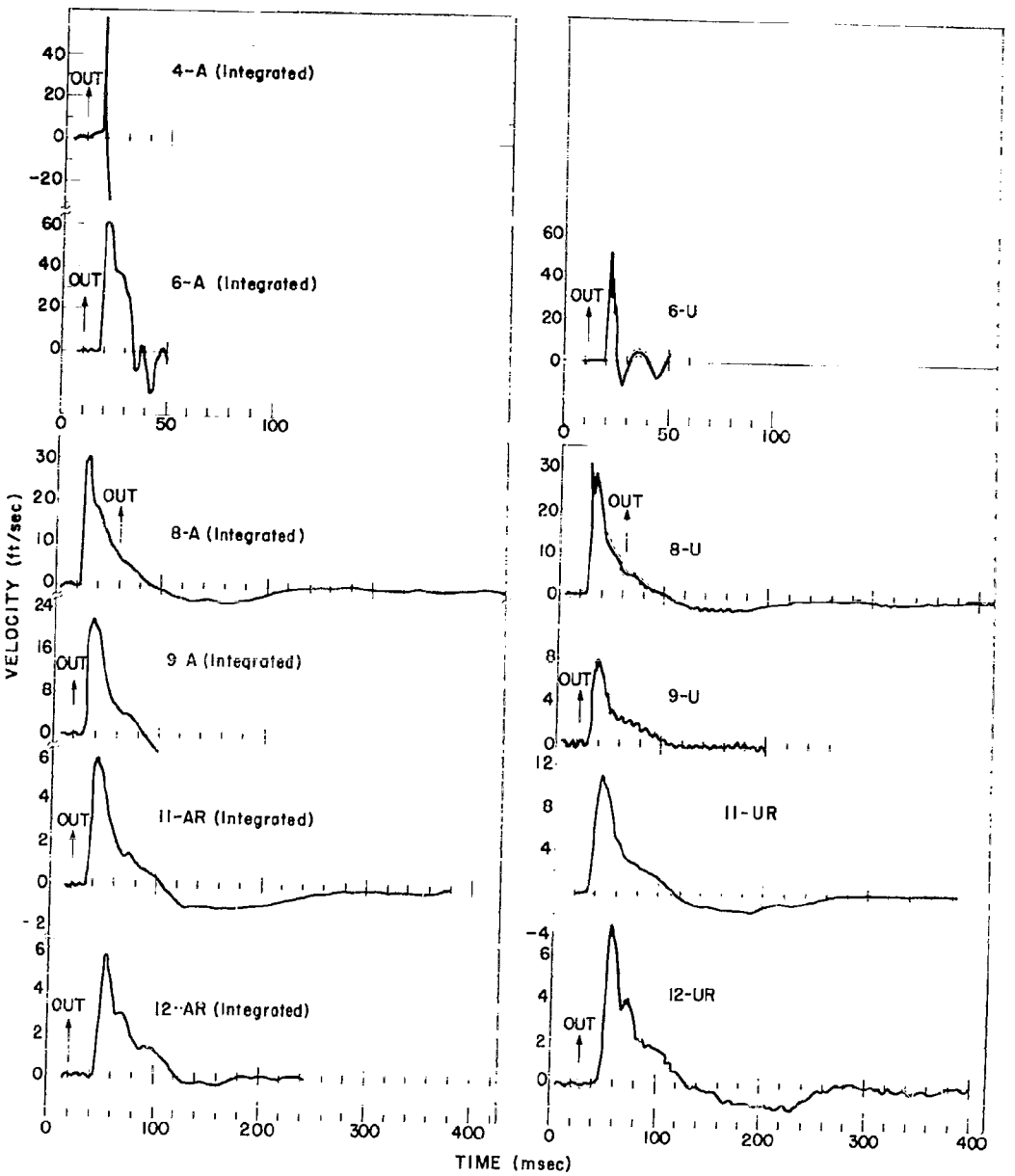

Figure 4.2 Radial particle velocities, Borings 4 through 12.

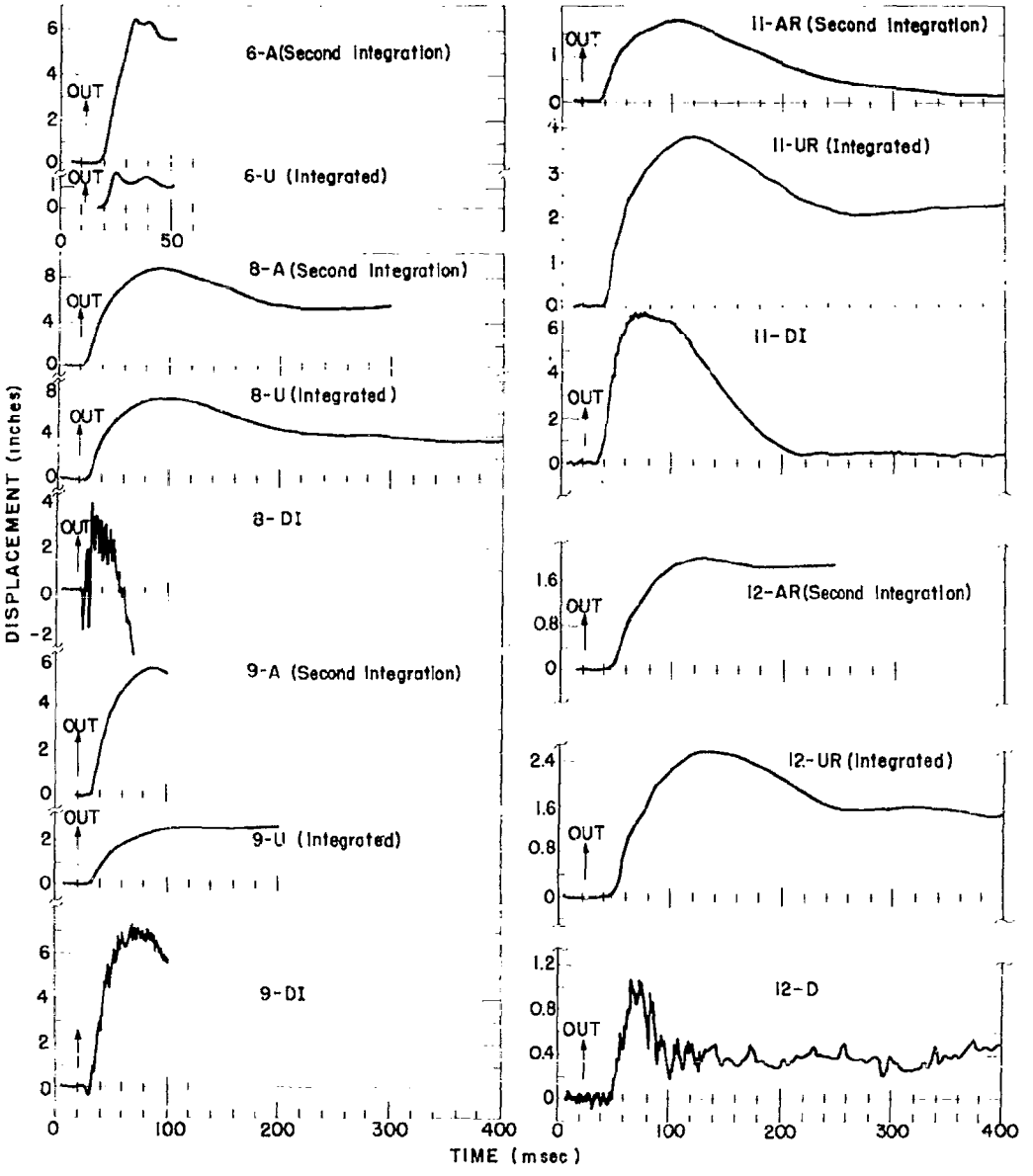

Figure 4.3 Radial displacements, Borings 4 through 12.

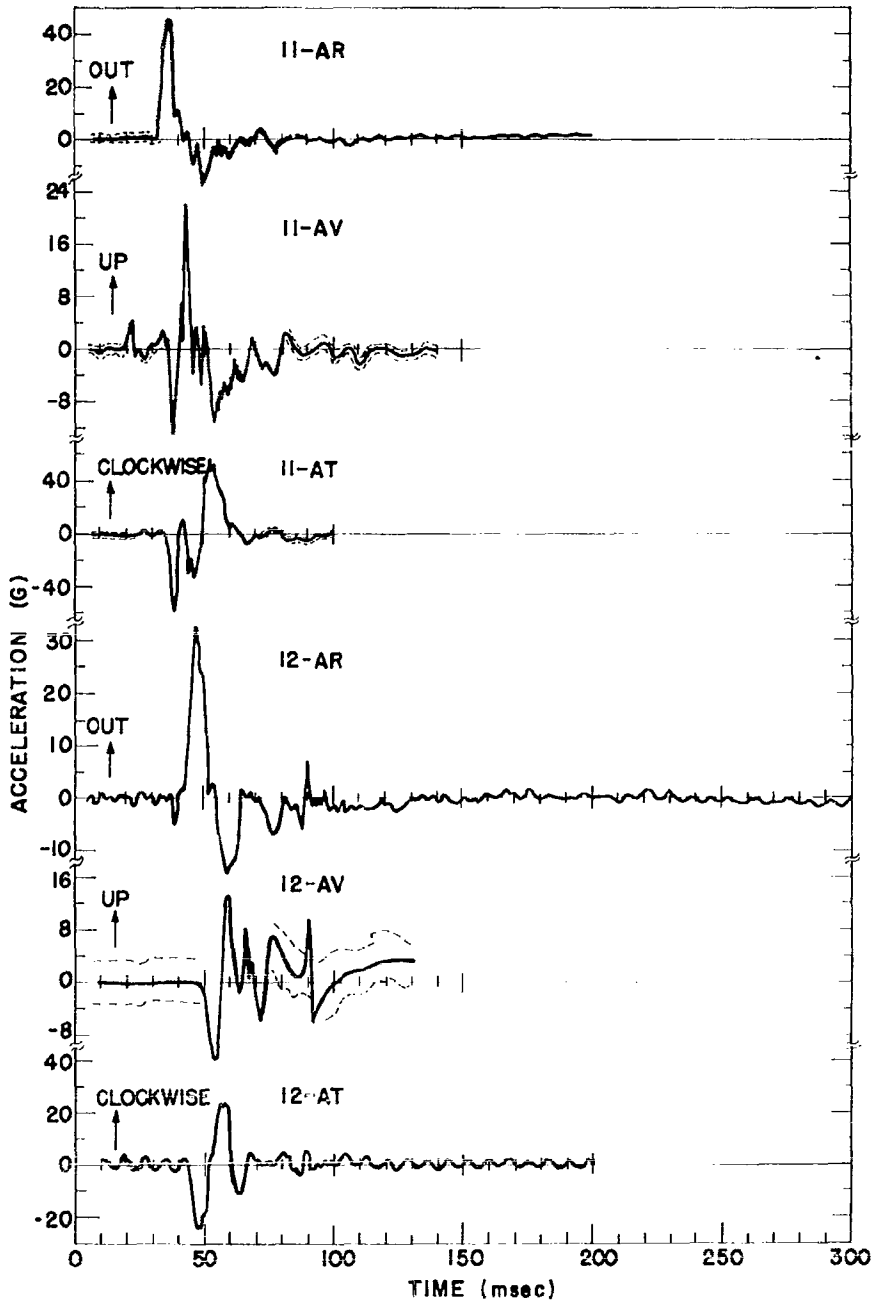

Figure 4.4 Radial, vertical, and tangential accelerations, Borings 11 and 12.

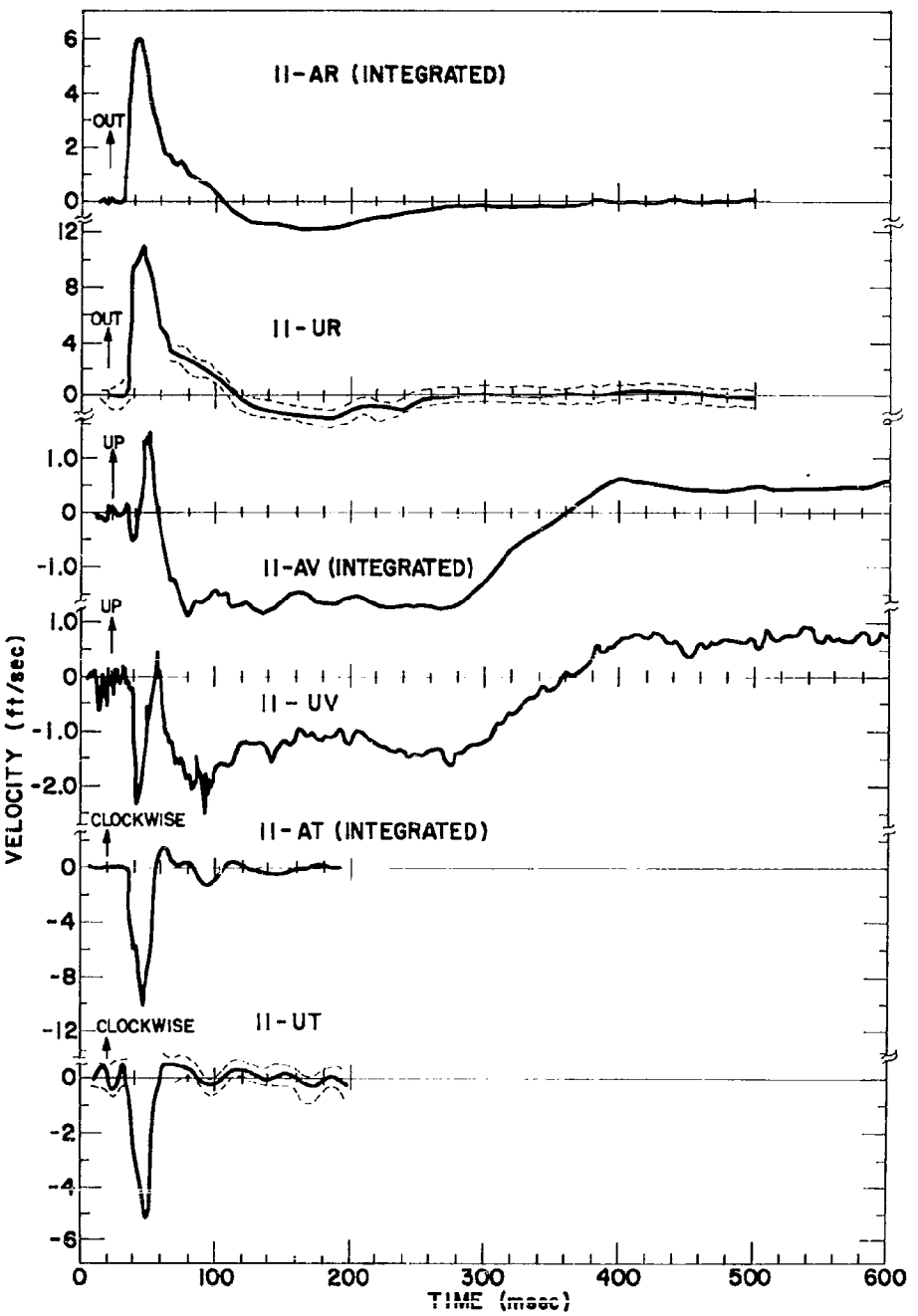

Figure 4.5 Radial, vertical, and tangential particle velocities, Boring 11.

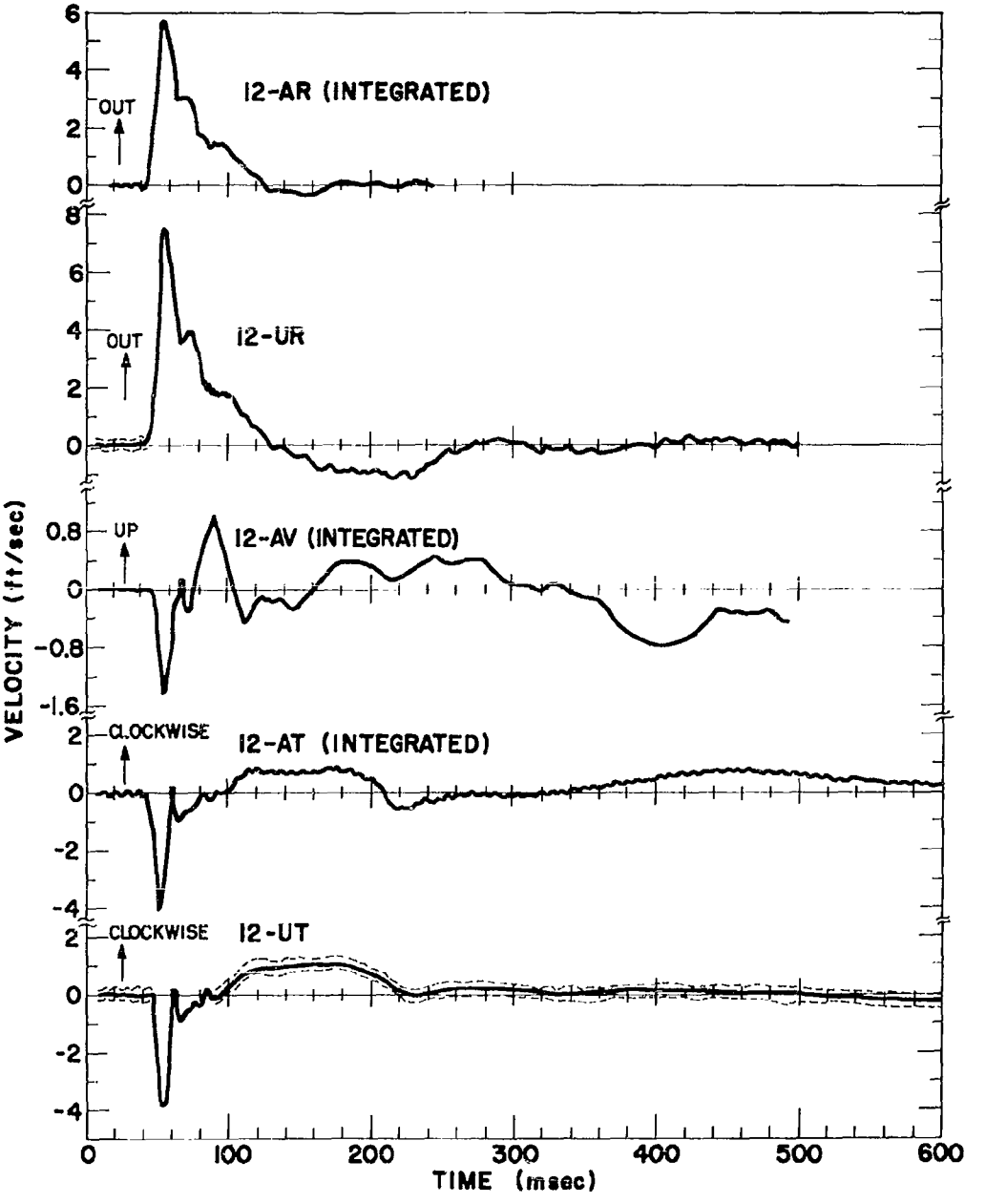

Figure 4.6 Radial, vertical, and tangential particle velocities Boring 12.

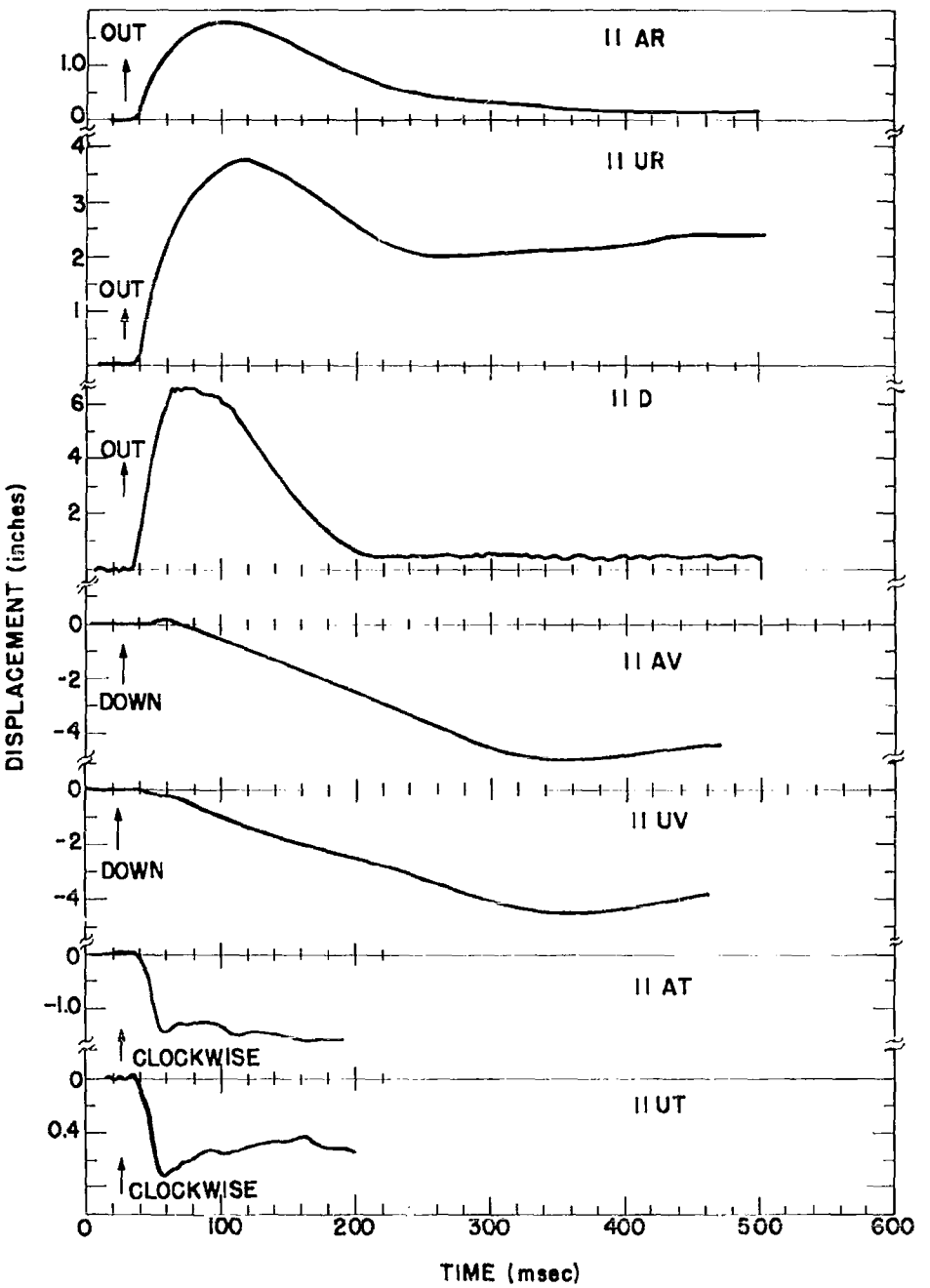

Figure 4.7 Radial, vertical, and tangential displacements, Boring 11.

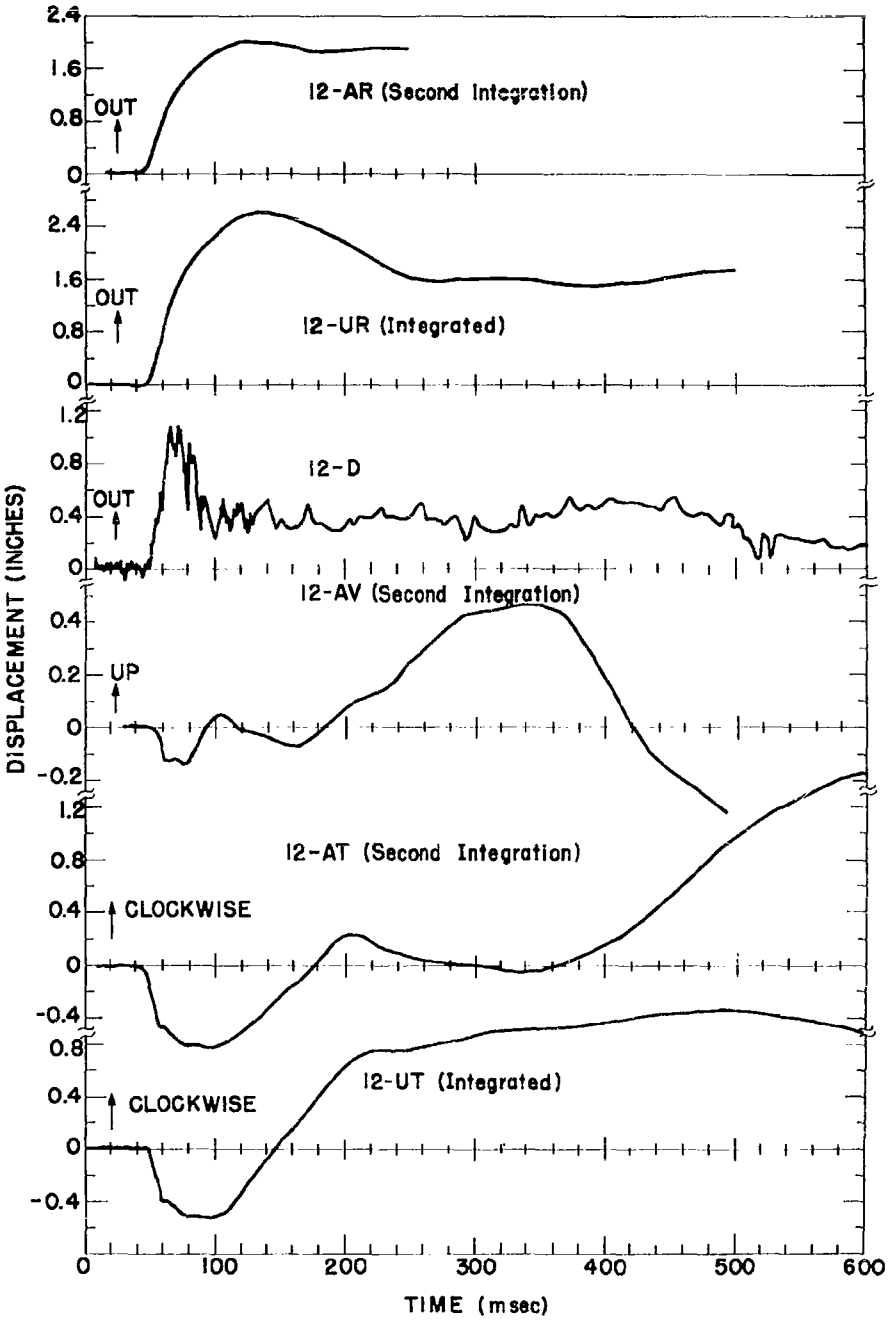

Figure 4.8 Radial, vertical, and tangential displacements, Boring 12.

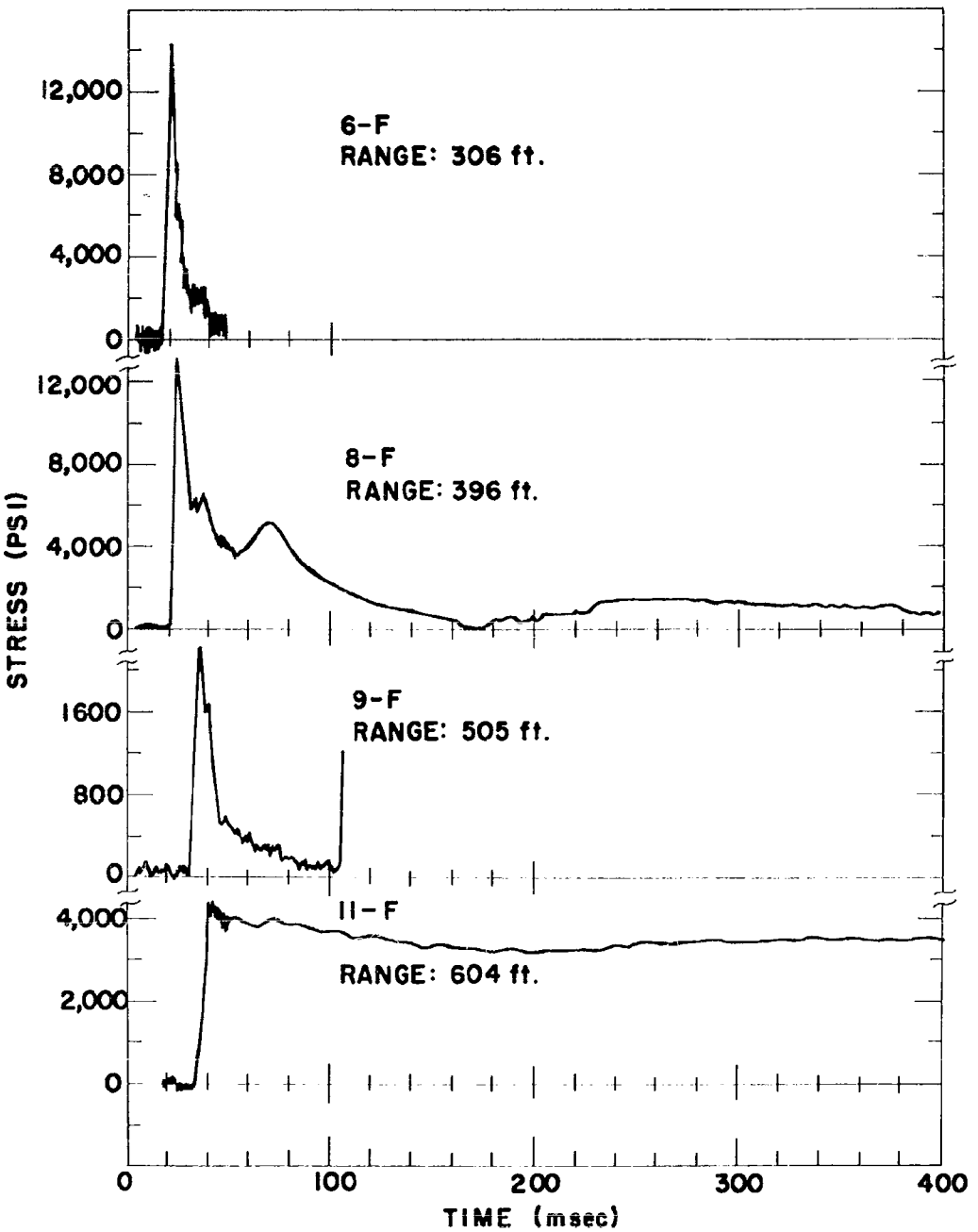

Figure 4.9 Radial stress, Borings 6, 8, 9, and 11.

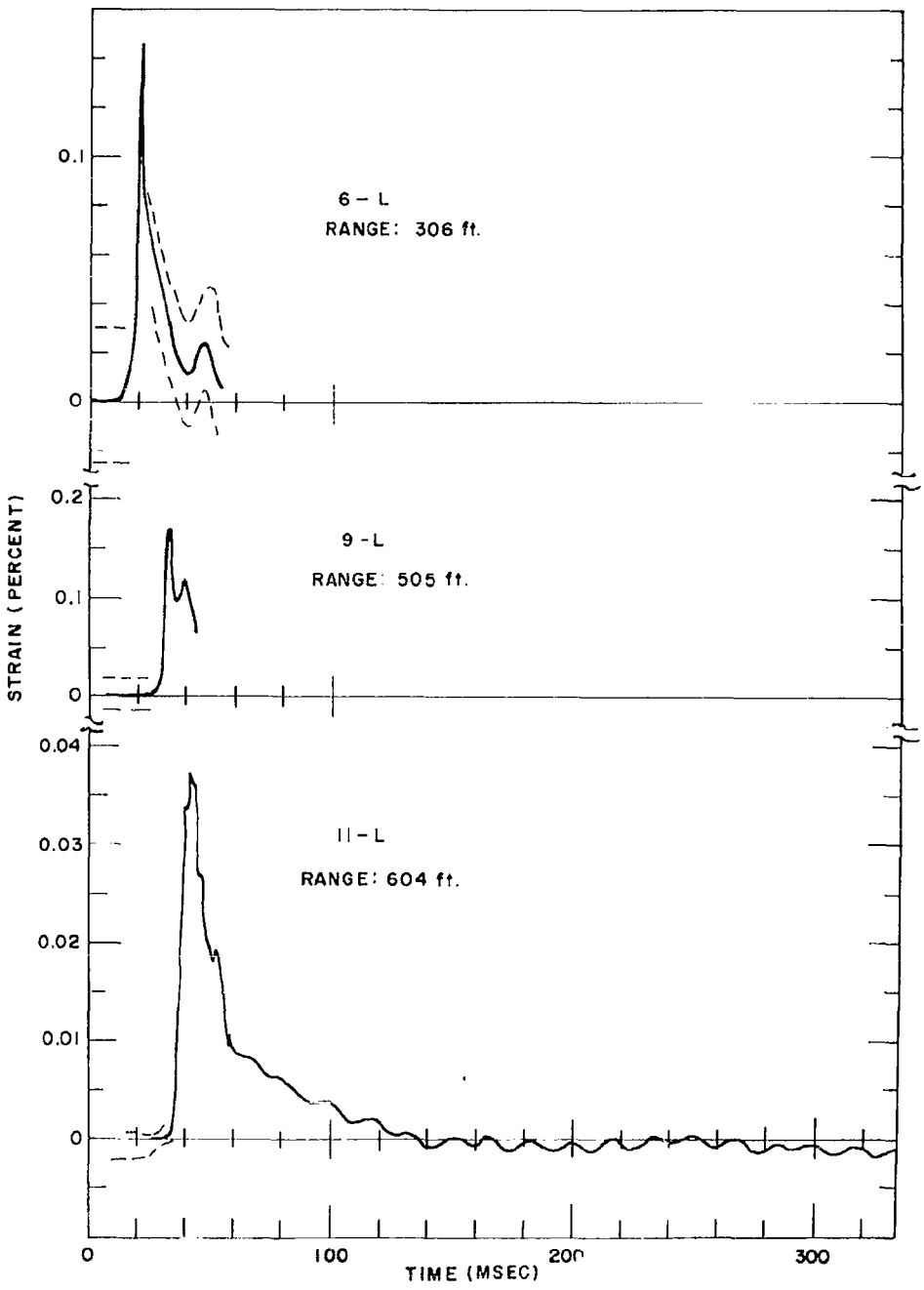

Figure 4.10 Radial strain, Borings 6, 9, and 11.

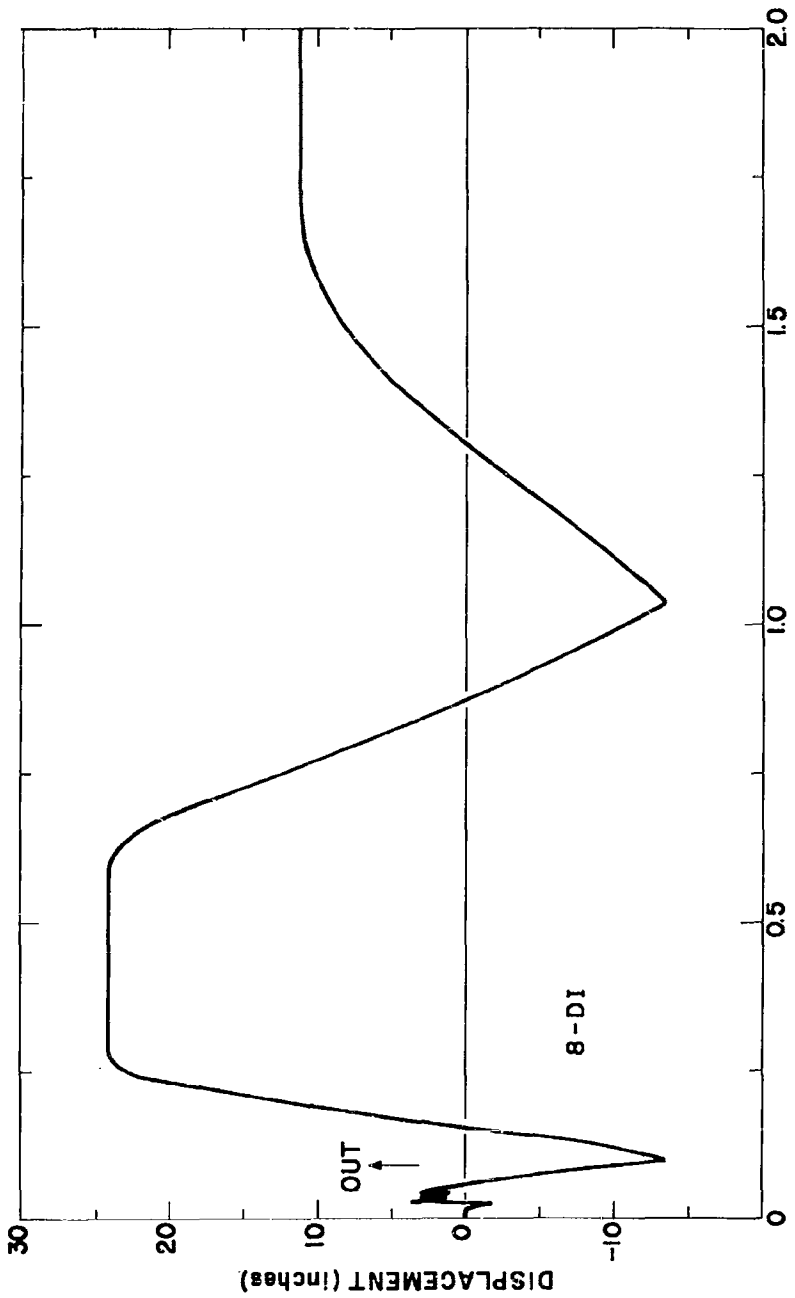

Figure 4.11 Inertial displacement record, Boring 8.

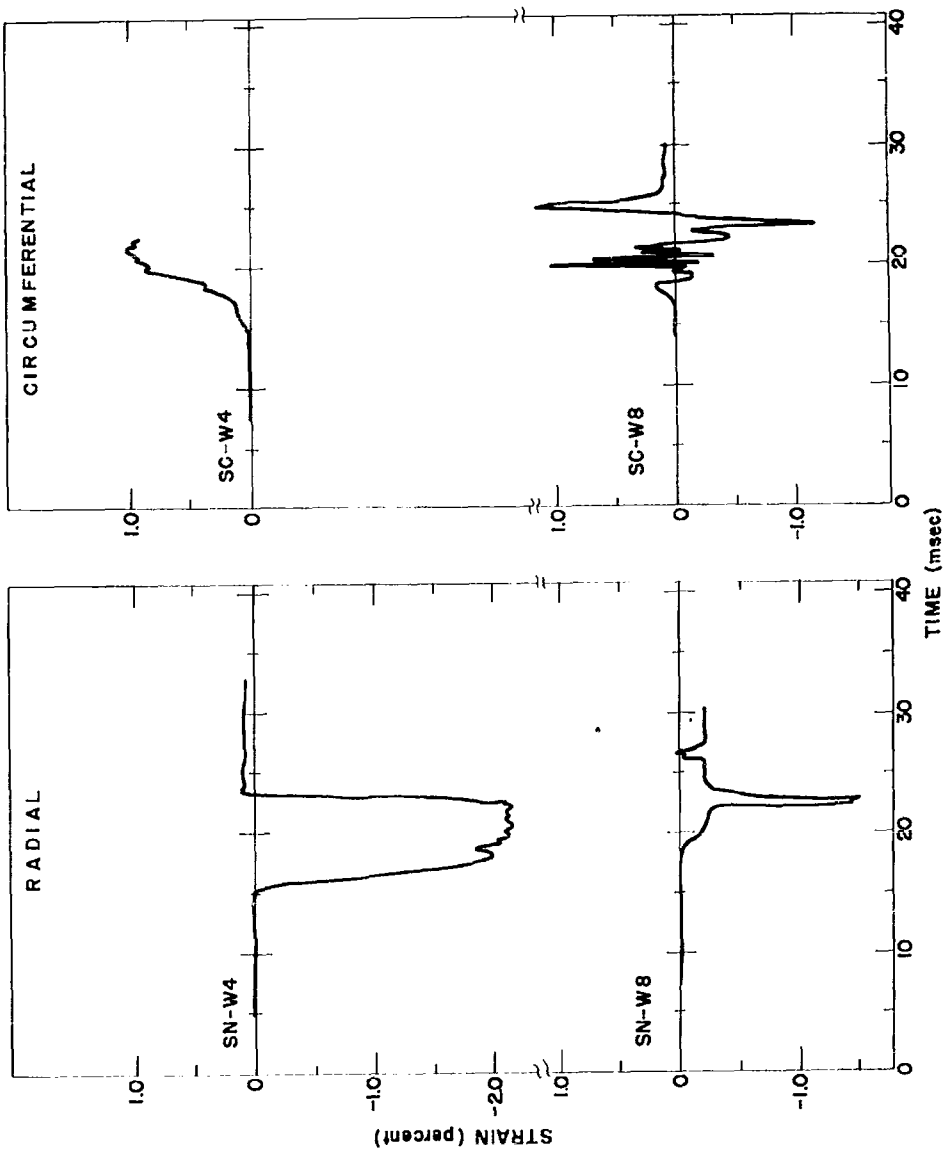

Figure 4.12 Strain records, Section SS, wall gages.

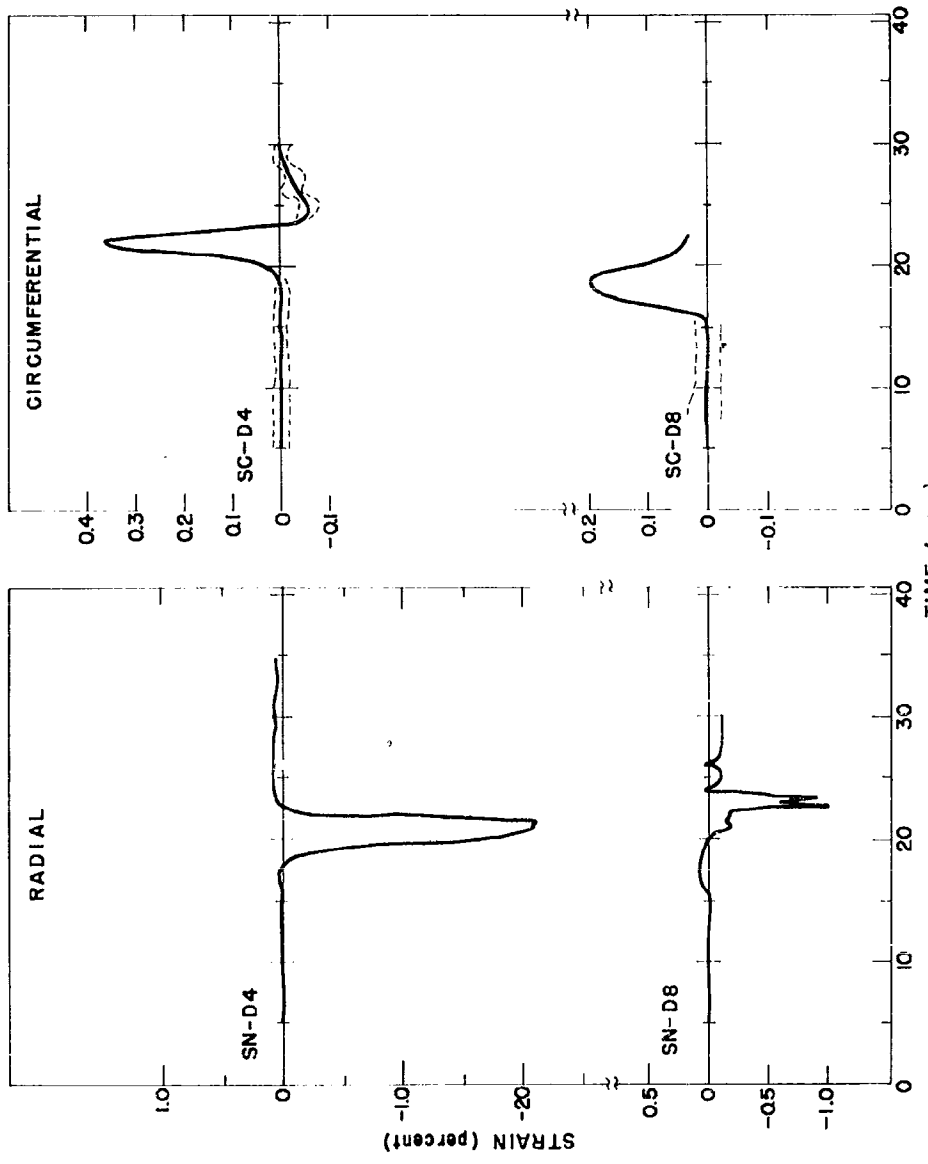

Figure 4.13 Strain records, Section SS, diagonal gages.

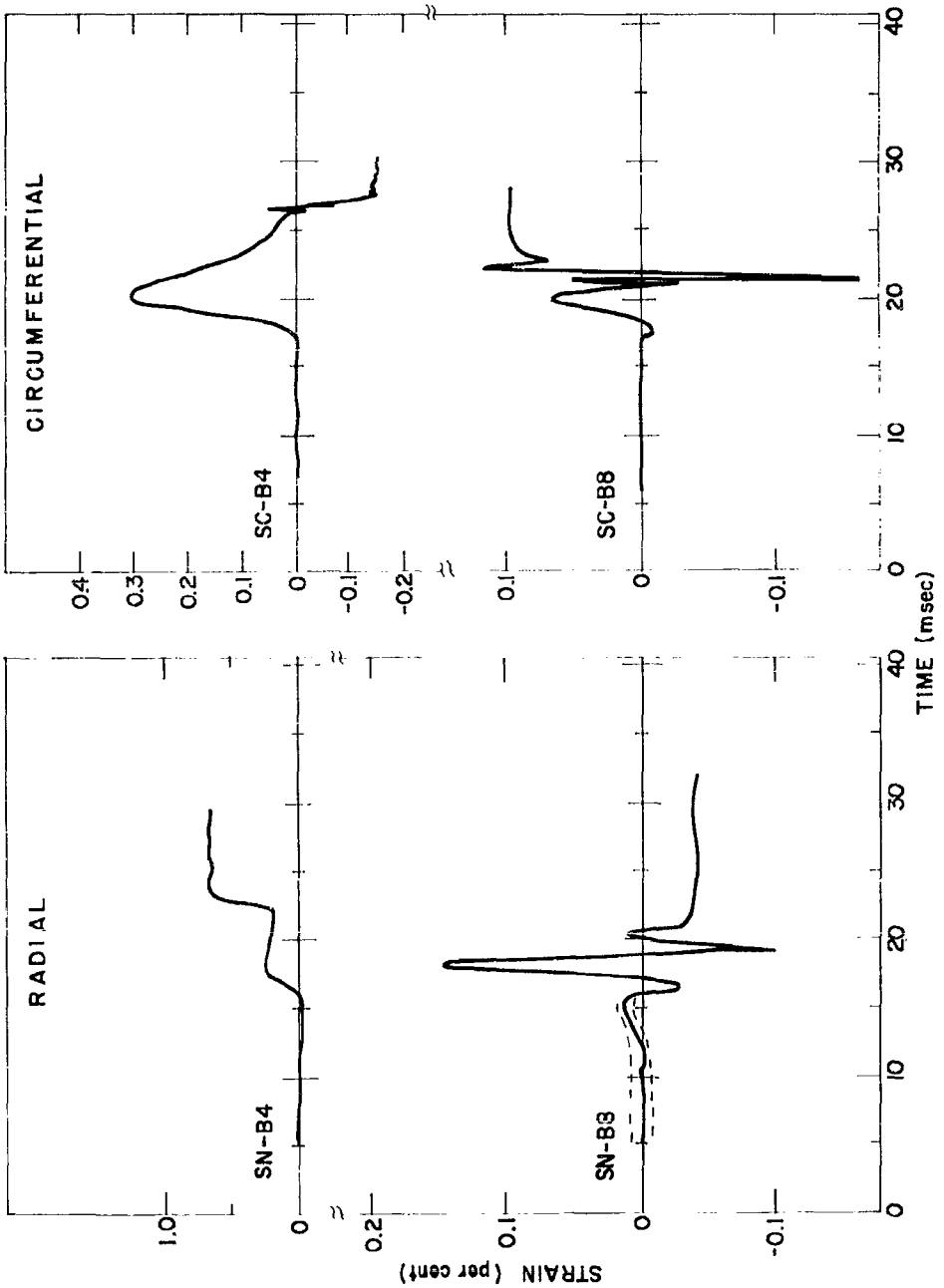

Figure 4.14 Strain records, Section SS, floor gages.

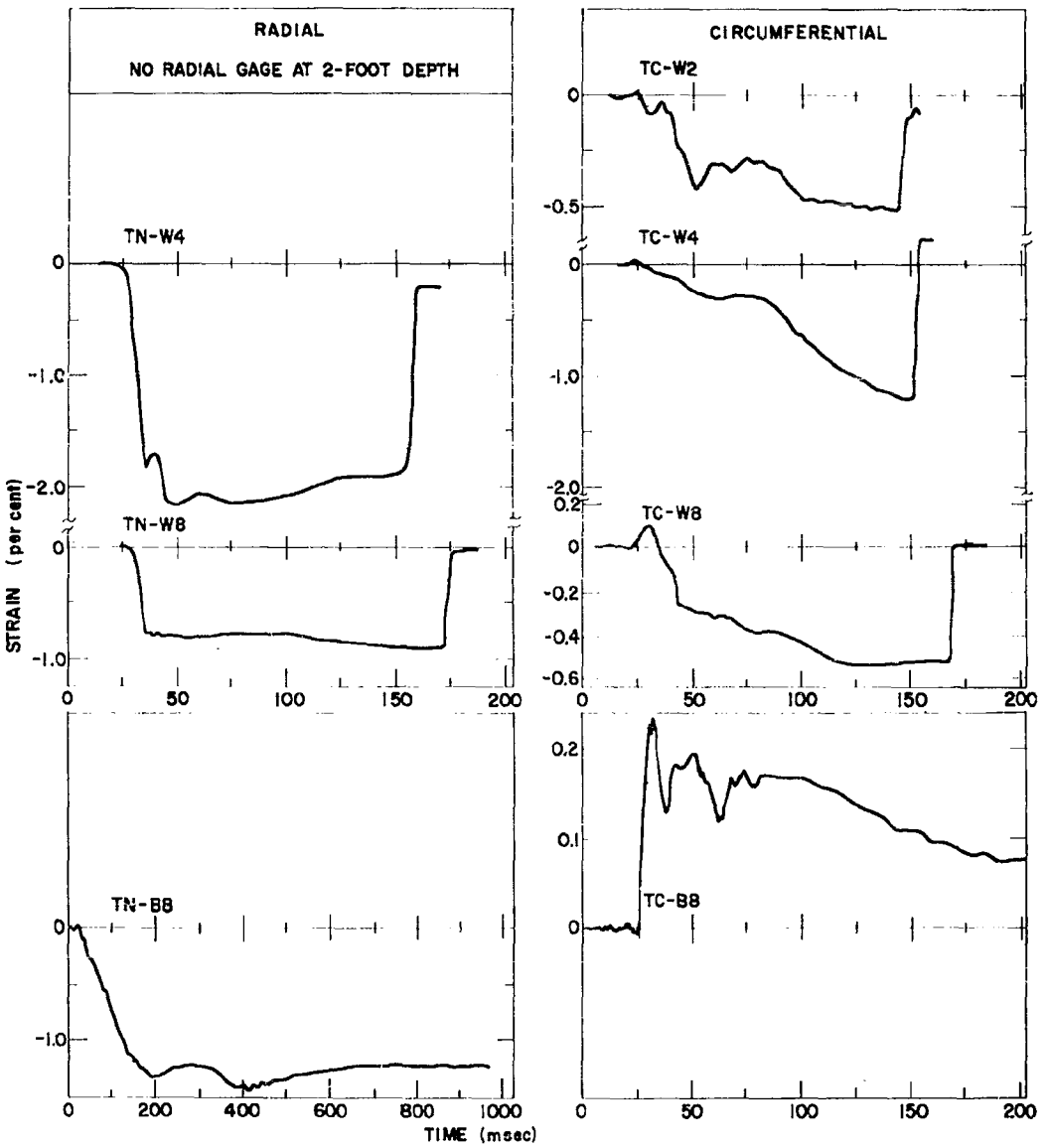

Figure 4.15 Strain records, Section TT, wall and floor gages.

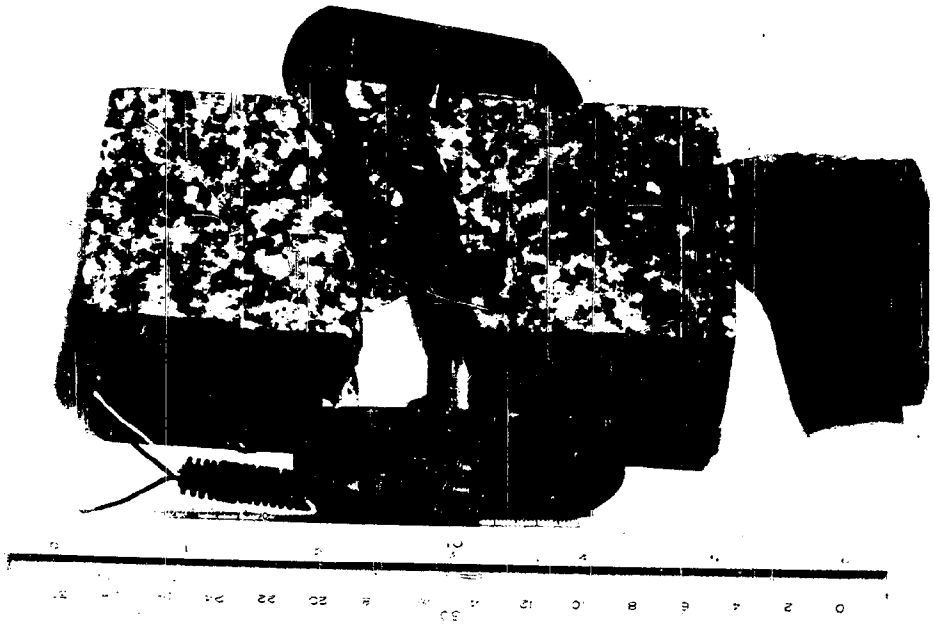

Figure 4.16 Strain gage and core TC-W2 after recovery.

Chapter 5

ANALYSIS AND DISCUSSION OF DATA

5.1 PROPAGATION VELOCITY

The velocity with which shock from the Hard Hat explosion was transmitted through granite to the gages of Project 3.3 may be derived from arrival-time data for the radial accelerometers. These gages are chosen because acceleration rise times are generally shorter than those of other motion parameters and initial motion is more readily determined. Velocities may be derived from travel times and distance from the source to each gage or from travel time and range differences between gages. The former process tends to smooth out effects of local anomalies but includes unusually high velocities within the hydrodynamic domain. The second procedure emphasizes local anomalies. The average velocity derived from a group of instruments by either procedure should be nearly the same.

Travel-time data are plotted versus range in Figure 5.1 and are listed in Table 5.1. Velocities computed by elapsed time and interval methods are included in the table. Average velocities by both methods differ by only about 1.2 percent; maximum deviation of the elapsed time data from the average is only 1.7 percent. The table shows the best average velocity to be 18,128 feet per second, with a standard deviation of 177 feet per second, or less than 1 percent.

The low velocity between stations at 255 and 306 feet suggests there is bad rock in this interval. A portion of a geological map of the tunnel developed by the Geological Section of Lawrence Radiation Laboratory, Nevada, is reproduced in Figure 5.2. This shows that the collar of Boring 6 lies within a group of shear zones which cross the tunnel axis at acute angles and include an appreciable portion of the interval between Borings 4 and 6. Dip of the shear zones implies that at gage level at least some of this incompetent rock lies between gages 4-A and 6-A.

5.2 PARTICLE ACCELERATION

Data presented in Table 4.1 indicate that accelerations decrease from 4226 g at 256 feet range to 32.7 g at 784 feet. These data, plotted in Figure 5.3 on logarithmic scales, show some scatter from a linear relation between acceleration and range, and only data from the 784-foot station suggests a break in slope. This is insufficient ground for defining a slope change. A least-square fit to these data (dashed line in the plot) shows attenuation of peak acceleration with the inverse 4.59-power of radial range. However, Stanford Research Institute has reported (Reference 5) for Project 1.2 an acceleration peak of 5.9 g at 1,500-foot range on a radius sloping downward about 50 degrees from the burst point on the same azimuth as the Project 3.3 instrumentation. This point is plotted in Figure 5.3, open symbol, and permits a more meaningful analysis. Least-square linear curves have been fitted for two sets of data. That for data between 256- and 604-foot ranges indicate attenuation as the inverse 5.12-power of radial range and that for data

from 604 to 1500 feet indicate attenuation as the inverse 2.92-power of range. The equations which express these relationships are:

$$a = 9.89 \times 10^{15} R^{-5.12 \pm 0.26} \qquad (5.1)$$

for ranges from 256 to 604 feet; and

$$a = 7.18 \times 10^{9} R^{-2.92 \pm 0.27} \qquad (5.2)$$

from 604 to 1500 feet. In both equations acceleration is in g-units and range in feet.

It has been mentioned that the record for gage 4-A implies that indicated peak acceleration may be low. However, analysis of all acceleration, as presented in Figure 5.3, suggests that it is not more than 4 percent below the value derived from Equation 5.1.

Variable rock conditions probably account for most of the scatter in data, which is characterized by an average deviation from the best-fit lines of not more than 13 percent.

5.3 PARTICLE VELOCITY

Particle-velocity data were derived by integration of acceleration-time data and by direct observation of velocity gage signals. Curves of radial component of particle velocity versus time are assembled in Figure 4.2, and peak values from these data are included in Table 4.1.

A plot of peak particle velocity versus radial range is presented in Figure 5.4. Data from two Project 1.2 stations, at 1500-foot range, have been added (open symbols). One of these stations, responsible for the two lower values, was on the downward sloping radius; the other was on a

horizontal radius at the same azimuth as Project 3.3 stations. These Project 1.2 data have been considered in the following analysis because they aid in determining a break in slope near 700 feet, which cannot be defined from Project 3.3 data alone. Because the data from the sloping radius are lower than those from the horizontal-radius gages, they are given less weight in the curve-fitting analysis. Also in this analysis, the peak velocity derived from Gage 4-A has been ignored, since cable damage in this channel evidently occurred so near the peak that a proper decay portion of the acceleration peak was not recorded and the integrated data are obviously spurious (note Figures 4.1 and 4.2).

Analysis of Project 3.3 velocity data shows attenuation of peak particle velocity at a rate indicated by the inverse 2.41 power of radial range between 306 and 784 feet. Inclusion of Project 1.2 data indicated that, between about 700 and 1500 feet, peak particle velocity u in feet per second is attenuated as the inverse 1.10-power of radial range in feet. These attenuation patterns are given by the following equations:

$$u = 5.32 \times 10^{7} R^{-2.41 \pm 0.23} \qquad (5.3)$$

between 306 and 730-foot range; and

$$u = 9.26 \times 10^{3} R^{-1.10 \pm 0.24} \qquad (5.4)$$

between 730 and 1500-foot range. Average deviation of data from these equations is about 18 percent.

The period of the velocity wave at each Project 3.3 station has been estimated by assuming that the decay time from peak to crossover in the first positive phase is one-quarter period. Periods so derived are plotted versus range in Figure 5.5. Rough readings from data curves published in Reference 5 indicate that at 1500 feet the period was about 260 milliseconds. It appears then that, beyond the region of nonlinear response, the particle velocity wave is propagated with a period of between 260 and 300 milliseconds.

Sharpe (Reference 6) has shown that application of a unit function of pressure within a cavity in an infinite elastic material will produce a wave the frequency of which is directly proportional to the propagation velocity within the medium and inversely proportional to the cavity radius. Nicholls, Hooker, and Duvall (Reference 7) in their report on dynamic studies of salt response in connection with Project Cowboy demonstrated that periods of strain oscillations were related to a cavity radius which corresponded to the mean radius of the zone of cracking or tensile splitting surrounding the explosion. Beyond this radius, rock response was elastic. They showed that the radius of this equivalent cavity, R_e, was given by the equation

$$R_e = (c\tau/2\pi)(1 - 2\nu)^{1/2}/(1 - \nu),$$

where c is seismic velocity, τ period, and ν is Poisson's ratio. The period of strain, pressure, and particle-velocity oscillations in rock responding within the elastic domain should be identical, and the elastic radius should be derivable from observed particle velocity periods.

The Project 9.5 report (Reference 8) gives a value of 0.27 for Poisson's ratio in Hard Hat granite, derived from compressional and shear wave velocities observed in situ. From these data the elastic cavity radius for Hard Hat, assuming an average period of 280 milliseconds, is found to be 750 feet.

The particle velocity attenuation curve plotted in Figure 5.4 indicates that velocity begins to decrease as approximately the inverse first power of range at 731 feet. Such an attenuation rate, 1/R, for particle velocity implies propagation under conditions of elastic or linear response. Under these conditions, energy in the wave front is being degraded only by spreading over the surface of the linearly expanding spherical wave and thus is decreasing as R^{-2}. Since energy is proportional to the square of particle velocity, the latter must decrease, under these conditions, as R^{-1}. Then the onset of inverse first power slope at 731 feet shows this to be the elastic radius, in excellent agreement with the corresponding quantity derived from velocity wave periods. The pressure computed from particle velocity at this change in slope is about 4600 psi, a reasonable value for the elastic limit of granite.

5.4 PARTICLE DISPLACEMENT

Particle displacement data are not so consistent as the acceleration data because integration is subject to considerable cumulative error and because the displacement gages have not yet been developed into reliable instruments. The data which are included in Table 4.1 are plotted versus

radial range in Figure 5.6. There is evidently more scatter among these data than among particle velocities. Several points are obviously wild and have been identified with question marks.

A least-square fit was established for displacement data, ignoring the points which have been questioned. The line drawn in Figure 5.6 is represented by the equation

$$\delta = 1.17 \times 10^{5} R^{-1.66 \pm 0.38},$$

where displacement, δ, is in inches, and range, R, in feet. Average deviation of the valid observed points from this expression is about 38 percent.

Residual displacements were derivable from some of the data. Gages in Boring 6 showed residuals of 86 and 93 percent of peak. In Boring 8, residuals were 61 and 48 percent of peak. Cable damage occurred too early at Boring 9 to permit observation of residual displacements. The records at Boring 11 gave residual displacements of 11, 39, and 7.5 percent of peak values. Boring 12 gages showed residuals 58 and 19 percent of peaks. Several displacement records, either derived by integration or observed directly, did not survive long enough or, as in the case of 8-DI, were influenced by motion other than translation so that residual data were meaningless. It is pertinent to note, however, that residual displacements decrease progressively outward through the nonlinear response region, from 90 percent of peak at 306-foot range to 20 percent of peak at 604 feet. The apparent increase at Boring 12 is probably introduced by data processing and gage response, and is not a real inversion in motion.

5.5 STRESS AND STRAIN

Data from stress and strain gages are considered together. Stress data were obtained from gages in Borings 6, 8, 9, and 11, and strains were observed at the same positions, except in Boring 8 where the strain gage failed before detonation. These data are plotted in Figure 5.7. It is evident from the plot that, at 505-foot range (Boring 9), stress is exceptionally low and strain high. It also appears that both stress and strain may be low at 306 feet, Boring 6. The lines drawn for stress and strain in Figure 5.7 are obviously based on a subjective estimate of the data and can only suggest the sort of attenuation which seem applicable.

It is of interest to perform certain computations on particle velocities and compare the results with observed stresses and strains. Conservation of momentum required that pressure or stress in a medium under dynamic load be equal to the product of density, particle velocity, and propagation velocity. Similarly, strain should equal the ratio of particle to propagation velocity. Thus, it should be feasible to derive stresses and strains from either the observed particle velocity data or from those computed by means of Equations 5.3 and 5.4. Furthermore, ratios of stress to strain are also of interest in comparison of observed with computed data. Results of such computations are presented in Table 5.2.

The computed stresses and strains obviously follow the particle velocity patterns, but it is evident that both stress and strain observed at 306 feet are about half the magnitude predicted from velocities. Observed stress at 396 feet is perhaps low by a factor of one-third. Absence of a

strain measurement does not permit further comment. The stress observed at 505 feet is abnormally low, perhaps one-fourth its anticipated value, and strain is about twice the expected magnitude. Particle velocity at this station is also about 50 percent greater than the curve implies. These anomalies are indicative of locally incompetent rock. Finally, at 604 feet, stress and strain are compatible with those derived from observed velocities.

The implication of this comparison of observed with computed stresses and strains is that neither gives a completely satisfactory indication of free field situation. This condition is in part the result of inhomogeneities in the environment, incompetent rock in relatively thick fault zones, in part the consequence of application of analytical methods based on linear response to data derived in a region of nonlinear response, and finally, the result of using experimental gages and mounting techniques.

The first of these factors, inhomogeneities, is illustrated by the results derived at the 505-foot station. Observed data are probably reliable there, at least in a qualitative sense. It is also apparent that, in a situation such as this one, stress and strain derived from particle velocity may be in error since here the material is so weak that the propagation velocity within the surrounding competent rock is not applicable and rock is so inelastic as to grossly affect even the peak stresses and strains.

Except in the case just discussed, non-linear response of the granite does not seem to have had sufficient influence on the peak particle velocity to have a serious effect on computed stresses. It seems likely that more serious consequences of non-elastic rock response will be evident in stress and strain records after the peak has been reached, i.e. stress decay will be more rapid than particle velocity decay and strain decay will be slower and some compressional strain may be residual.

Both stress and strain gages were experimental. At high stress levels it is very possible that stress gage elements may have become less sensitive than calibration implied. Strains measured in cores of the native rock grouted into borings may differ considerably from those in the rock in situ.

Stress-strain ratios are remarkably consistent, with the exception of that for the observed stress and strain at 505 feet, which is 1.39×10^6 psi, lower by nearly an order of magnitude than all other computed values of the ratio. The average value of the ratio for all computed stresses and strains is 11.97×10^6 psi. The corresponding average for the observed stress and strain at Borings 6 and 11 is 10.66×10^6 psi. The modulus of elasticity quoted in Chapter 2 of this report from laboratory tests on cores from the Hard Hat site is 11.3×10^6 psi.

5.6 TRANSVERSE PARTICLE MOTION

Particle motion transverse to the direction of shock propagation is indicative of asymmetry either in the source or in the environment. At each of the two most distant stations of Project 3.3, both accelerometers

and velocity gages were installed to respond to vertical and tangential (horizontal) components of motion. Records from gages 11-AV, 11-AT, 11-UV, 11-UT, and the corresponding Boring 12 gages, presented in Figures 4.5 through 4.8, show that there was significant asymmetrical transverse motion at both stations.

Initial vertical acceleration and particle velocity at both stations was downward, followed in both cases by a strong upward motion. Initial tangential acceleration and velocity at both stations was counterclockwise. These gages showed no appreciable clockwise velocity except for some long-period low-amplitude signal in the 12-AT and 12-UT records.

Displacements at these two stations are represented by hodographs in Figures 5.8 through 5.13. These curves follow the motion in the vertical-radial, vertical-tangential, and radial-tangential planes for both stations. Numbers on the curves adjacent to circled points are times in milli-seconds after detonation. These hodographs are good representations of motion through the first 200 milliseconds after detonation, but for longer periods, particularly in the tangential component at Boring 12, they are probably not very reliable because of the cumulative errors intro-duced by integration. Similarity in shape of displacement curves from accelerometers and velocity gages (Figure 4.8) indicates that, except for differences in amplitudes, displacement hodographs from velocity-gage data are very similar to those presented above.

The hodographs indicate a marked one-sidedness of motion and similarity of motion at Borings 11 and 12. In general terms, the motion was out, then down and counterclockwise. It seems probable that local slippage in several of the shear zones may account for the peculiarity of motion observed. It must be noted, however, that termination of some of the records as early as 200 milliseconds excludes knowledge of possible later movement.

5.7 COMPARISON OF GROUND MOTION IN VARIOUS ROCK ENVIRONMENTS

It seems pertinent to compare the results of analysis of Hard Hat free-field data with those of similar analyses of data obtained in other rock environments. Such comparisons are feasible for salt, tuff, and desert alluvium using data from the Gnome (Reference 9), Rainier (Reference 10), Scooter (Reference 11), and Fisher and Hognose (Reference 12) underground explosions.

Data from all events used in this comparison have been converted by cube-root scaling to the Hard Hat yield, 5.9 kilotons. It is noted that Scooter was a cratering shot comprising 0.5 kiloton of TNT, and some of the data from it may not be directly comparable to data from contained nuclear explosions in desert alluvium. However, since the Scooter data comprise the only information from very close to an explosive energy source in desert alluvium, it seemed pertinent to include it with the Fisher-Hognose data. Comparison will be made using acceleration and particle velocity data only. Displacement data have generally included too much scatter to make significant comparisons.

Curves representing best fits to acceleration data for granite, salt, tuff, and alluvium are included in Figure 5.14. These curves indicate a strong similarity in response of the hard rocks, granite and salt, and corresponding similarity of response in friable, porous rocks, tuff and alluvium. Rates of attenuation in similar materials are comparable, as are changes in slope, which are interpreted as changes in character of response of the material to shock loading. It is significant to note that, throughout

the region of rapid attenuation, peak accelerations in friable media are roughly two orders of magnitude less than accelerations in hard rock at the same radial range. Since peak accelerations are primarily a measure of the rate of rise or steepness of the pressure or velocity wave, the very great difference between peaks in hard, elastic rock and friable, porous rock implies that, at ranges less than the shortest included in Figure 5.14 (that is, before peak accelerations have fallen to 10^4 g) shock-front slopes have been rigorously degraded within the porous rock. This difference between shock-front slopes in the two types of material continues to the region where peak accelerations are roughly one g.

Particle velocity data from the same sources have been similarly represented in Figure 5.15 by least-squares curves. Here Scooter data appear to be higher than Fisher-Hognose data by a factor of about 5. This is consistent with the fact that a spherical TNT explosion in dry desert alluvium may be expected to propagate a shock wave in which peak pressure or particle velocity beyond the charge radius are greater than those from a nuclear charge of equal energy at the same radial range. This implies a greater efficiency for generation of pressure by the chemical explosive. The apparent discrepancy between this situation and the evident congruity of acceleration data from the two types of source simply emphasizes that peak accelerations in their dependence on wave-front slope are controlled by properties of the material traversed and not by peak pressures or velocities. The latter are strongly controlled by the nature of the explosion, as well as the traversed material.

Curves for porous rocks indicate a change in slope from $R^{-2.95}$ in tuff and $R^{-3.95}$ in alluvium to R^{-1} in the vicinity of 600 feet. As previously noted, this slope transition is interpreted as the onset of elastic or linear response of the rock to the shock wave. Peak pressures at these transitions may be computed from corresponding particle velocities, rock density, and propagation velocities on the basis of conservation of momentum across the shock front.

The tuff curve transition occurs at a particle velocity of 6.3 feet per second. Using a density of 1.9 and a propagation velocity of 8700 feet per second, the elastic limit for tuff under dynamic load is 98 bars or 1444 psi. Similarly, the elastic limit for desert alluvium, for which density is 1.6 and propagation velocity is 3500 feet per second, is found to be 3.2 bars or 47 psi.

The data from Hard Hat indicate the transition to linear response occurs at a range of 731 feet and a particle velocity of about 7 feet per second, which, for a density of 2.67 and propagation velocity of 18,128 feet per second, gives an elastic limit of 315 bars or about 4627 psi.

Particle-velocity data for salt show no break to R^{-1} slope but to an intermediate slope of $R^{-1.6}$, which may indicate a distinction between compressive crushing at ranges less than 370 feet where the slope transition occurs and tensile splitting or cracking beyond 370 feet. This transition occurs at about 60 feet per second which, for salt of density 2.2 and propagation velocity 14,500 feet per second, corresponds to a pressure of 1.78 kilobars, or about 26,000 psi. The salt data which extend to about

0.025 foot per second without breaking from the $R^{-1.6}$ slope imply that linear response has not developed out to that point, about 50,000 feet as scaled. This further implies that the elastic limit must be below 7.4 bars or 109 psi; a conclusion that seems hardly likely for this material.

TABLE 5.1 PROPAGATION VELOCITY

Range	Travel Time	Propagation Velocity by Elapsed Time	Propagation Velocity by Interval Time
ft	msec	ft/sec	ft/sec
256	14.1	18,150	18,150
306	17.1	17,900	16,670
396	22.0	18,000	18,360
505	28.0	18,030	18,180
604	33.0	18,260	19,800
784	42.5	18,430	18,950
Average	----	18,128	18,352

TABLE 5.2 STRESS AND STRAIN COMPARISONS

Range	Observed Velocities				Computed Velocities				Observed Stress and Strain		
	u_o	σ	ε	σ/ε	u_c	σ	ε	σ/ε	σ_o	ε_o	σ_o/ε_o
ft	ft/sec	psi	%	psi	ft/sec	psi	%	psi	psi	%	psi
306	60.6	40,056	0.33	11.99×10^6	55.3	36,560	0.31	11.99×10^6	14,036	0.15	9.36×10^6
	51.3	33,909	0.28	11.98×10^6							
396	30.1	19,896	0.17	11.99×10^6	29.7	19,625	0.16	11.97×10^6	13,051	-	-
	30.0	19,380	0.16	12.02×10^6							
505	21.4	14,145	0.12	11.99×10^6	16.5	10,913	0.09	11.99×10^6	2,230	0.16	1.39×10^6
604	5.97	3,946	0.033	11.96×10^6	8.31	5,506	0.046	11.97×10^6	4,423	0.037	11.95×10^6
	11.0	7,271	0.061	11.92×10^6							
784	5.7	3,768	0.031	12.16×10^6	6.26	4,138	0.035	11.82×10^6	-	-	-
	7.42	4,905	0.041	11.96×10^6							

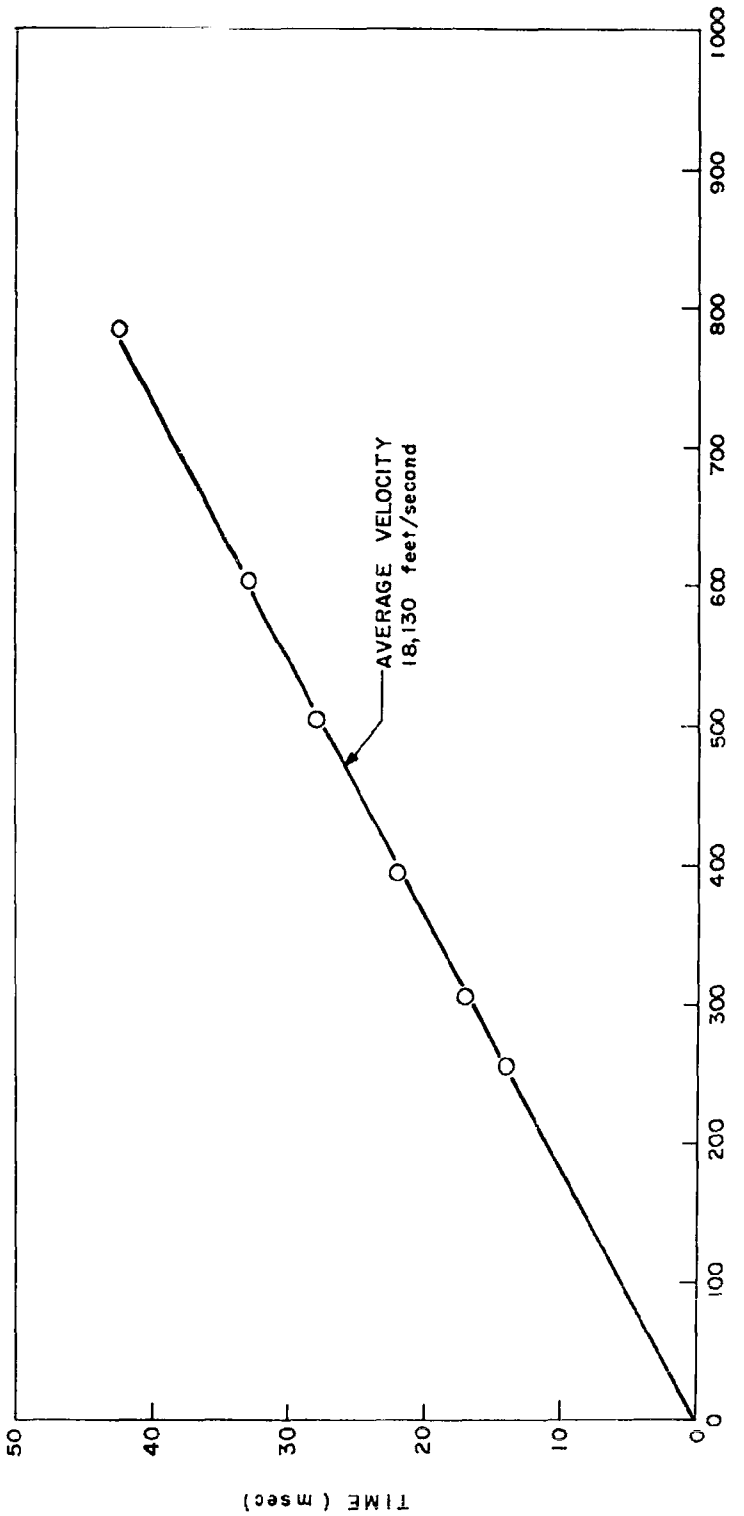

Figure 5.1 Travel-time curve, Project 3.3 instrumentation.

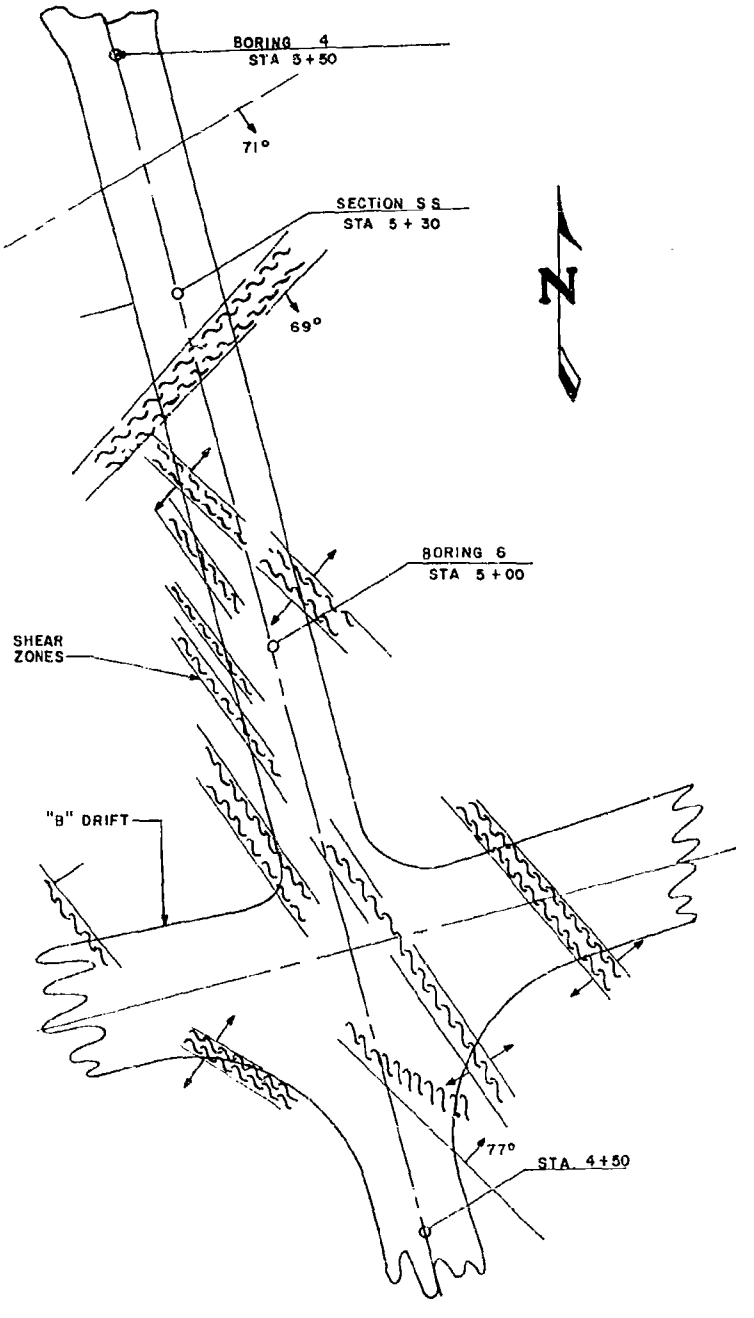

Figure 5.2 Geological map of part of Hard Hat access tunnel.

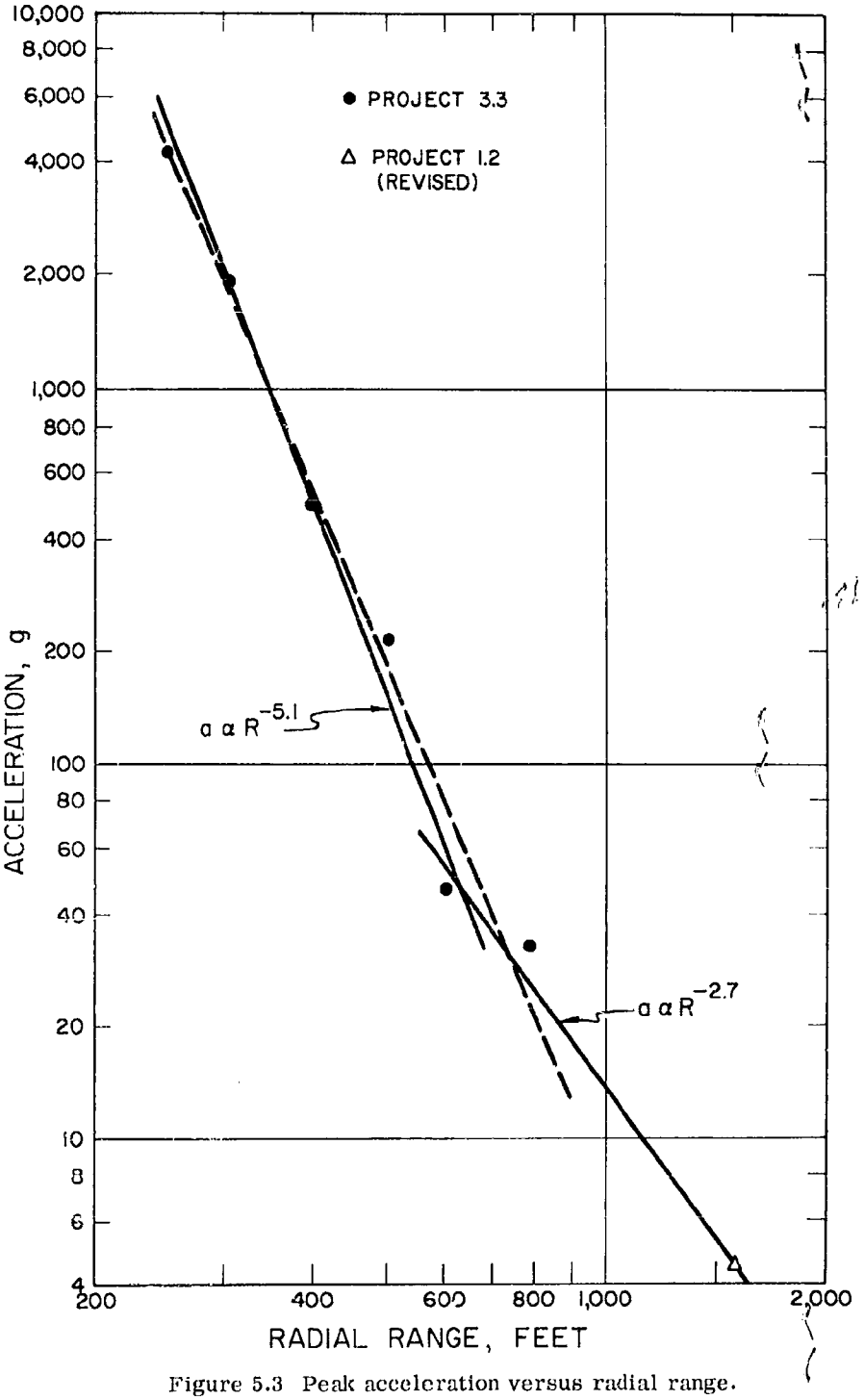

Figure 5.3 Peak acceleration versus radial range.

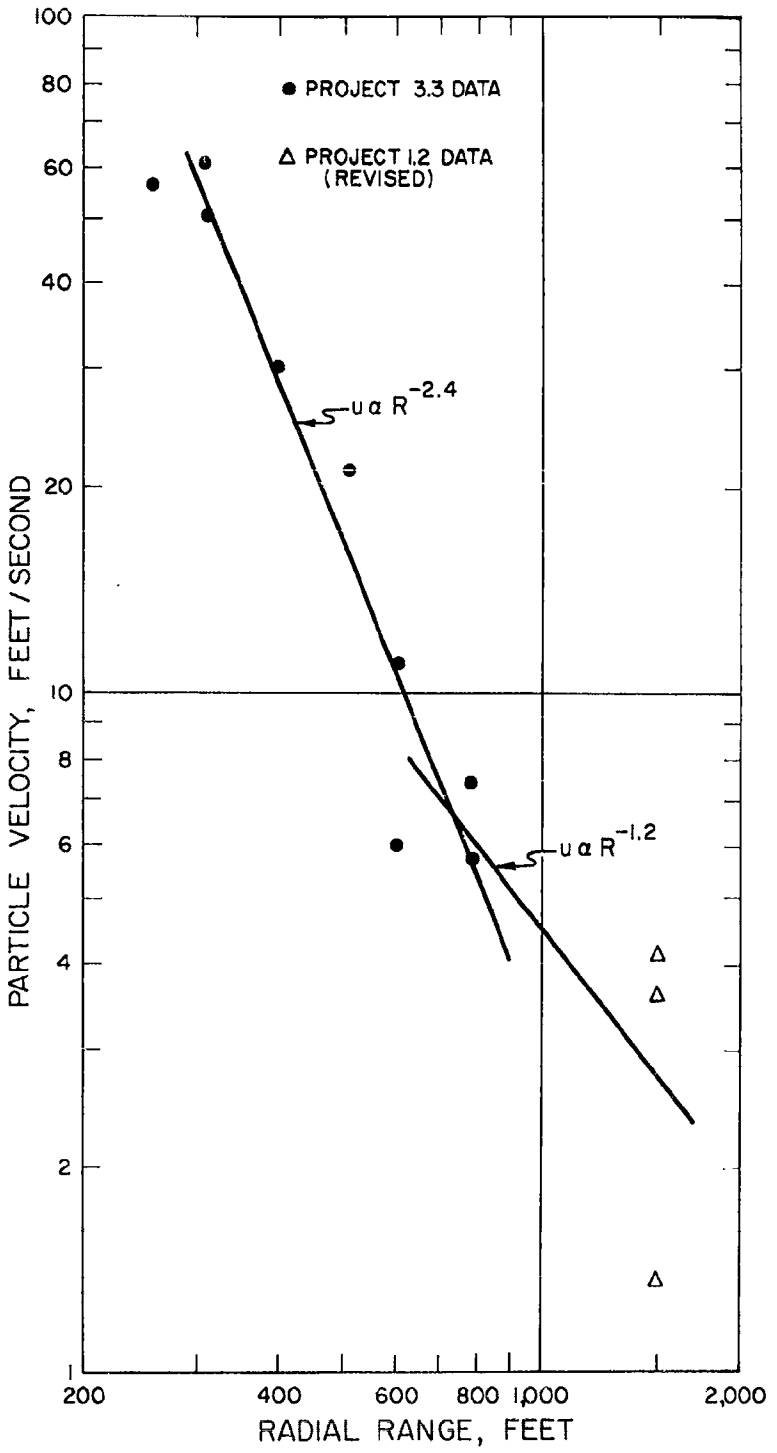

Figure 5.4 Peak particle velocity versus radial range.

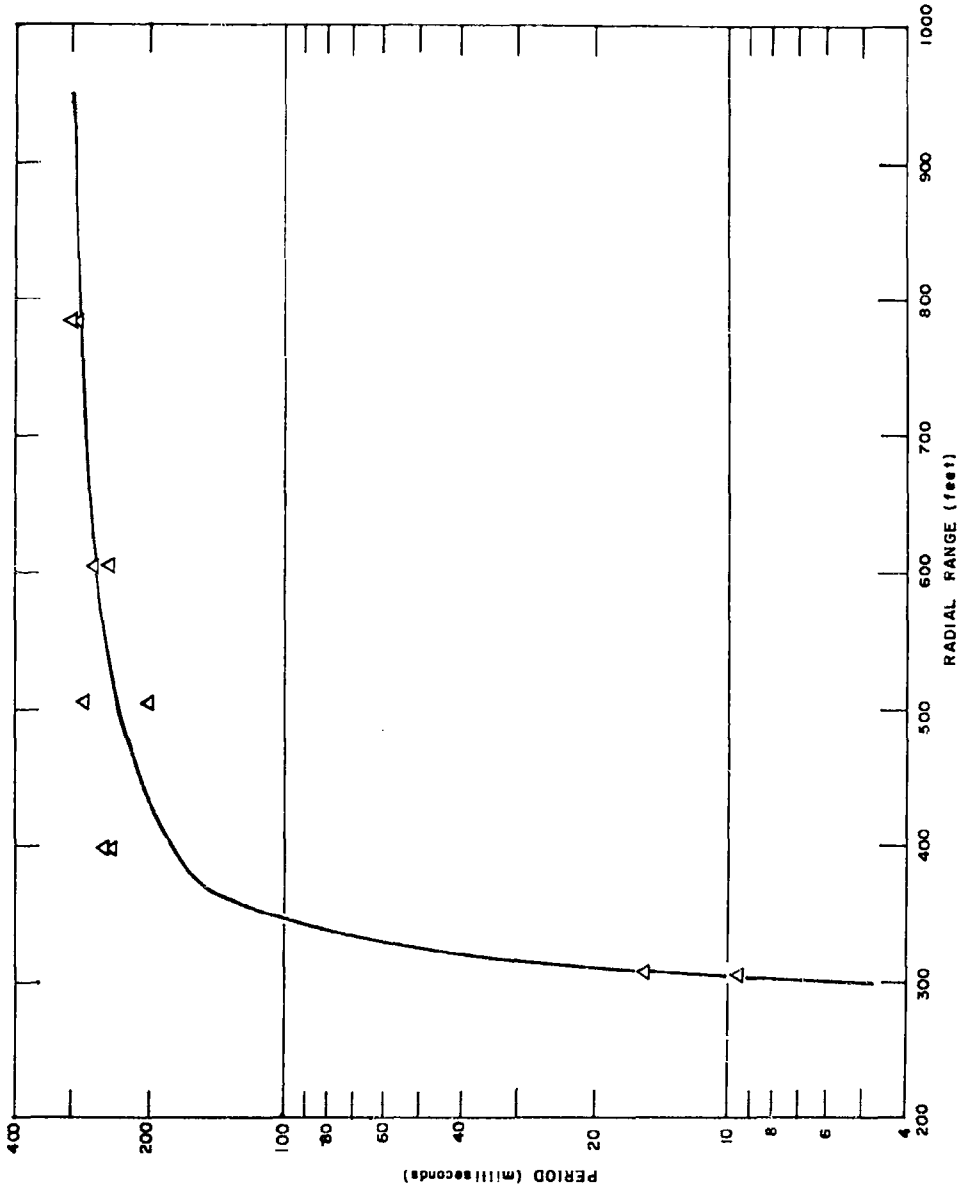

Figure 5.5 Particle velocity period versus radial range.

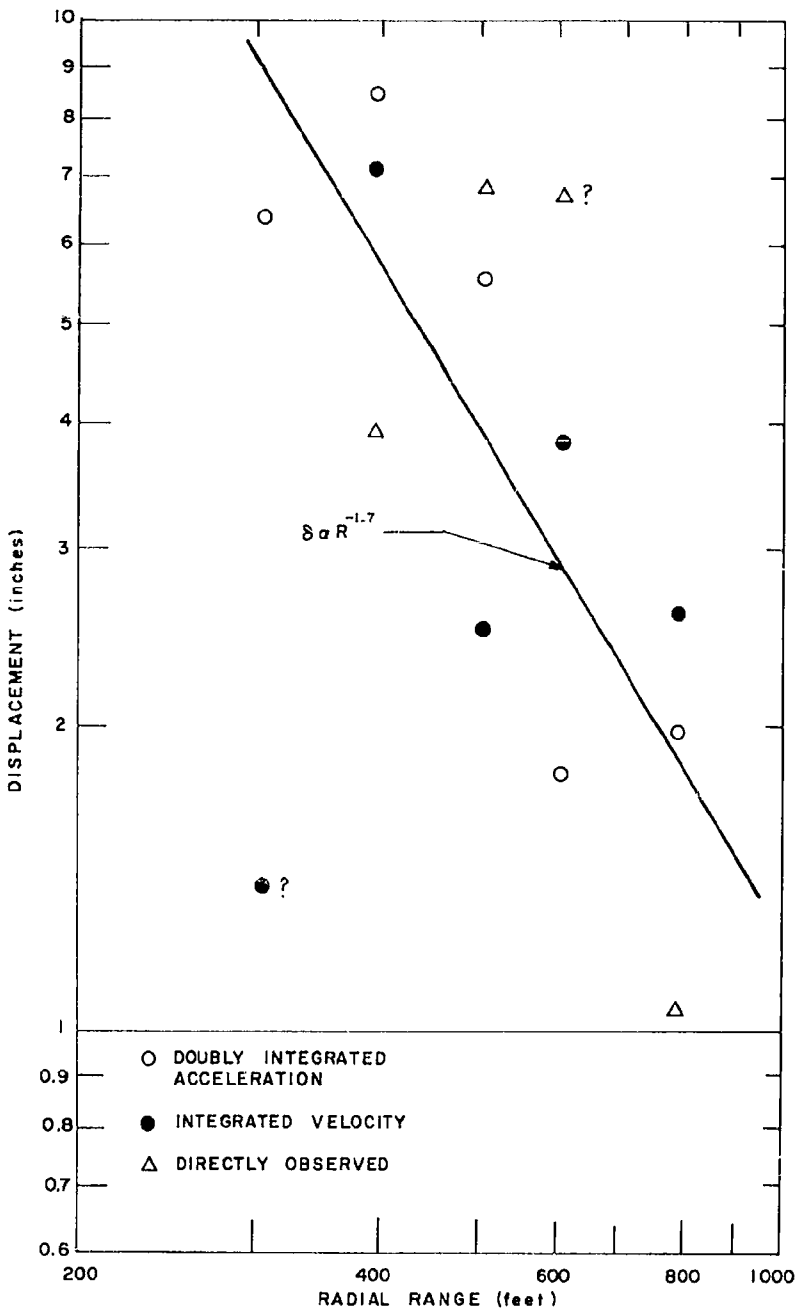

Figure 5.6 Particle displacement versus radial range.

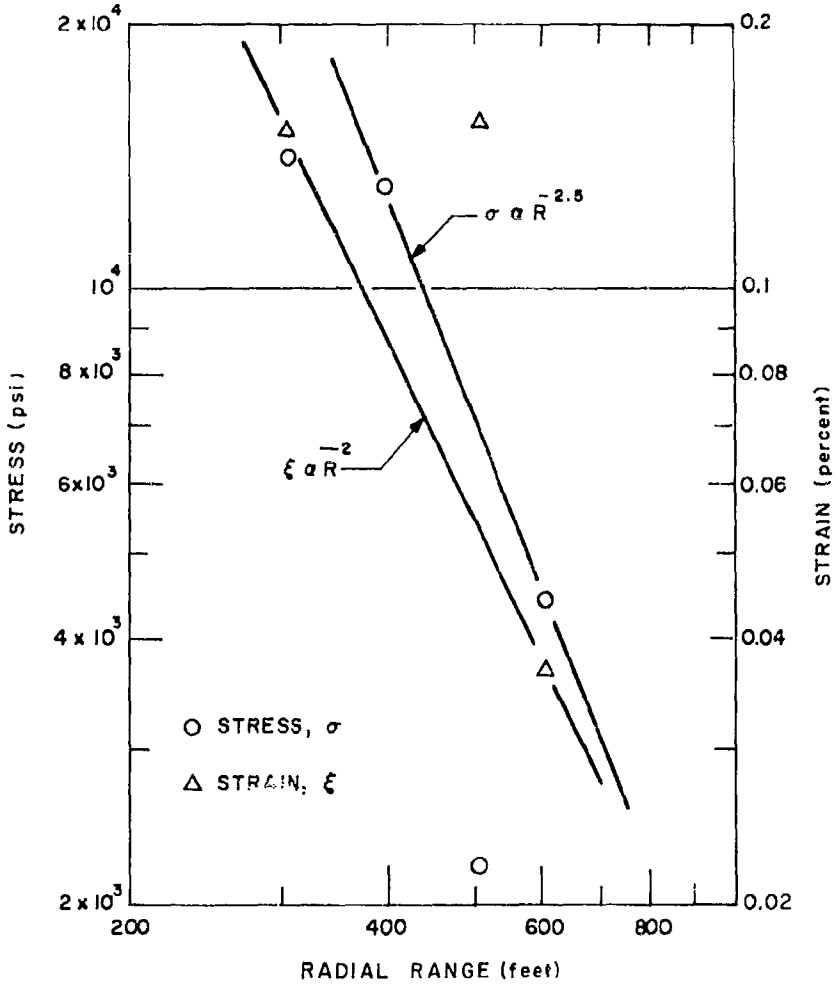

Figure 5.7 Stress and strain versus radial range.

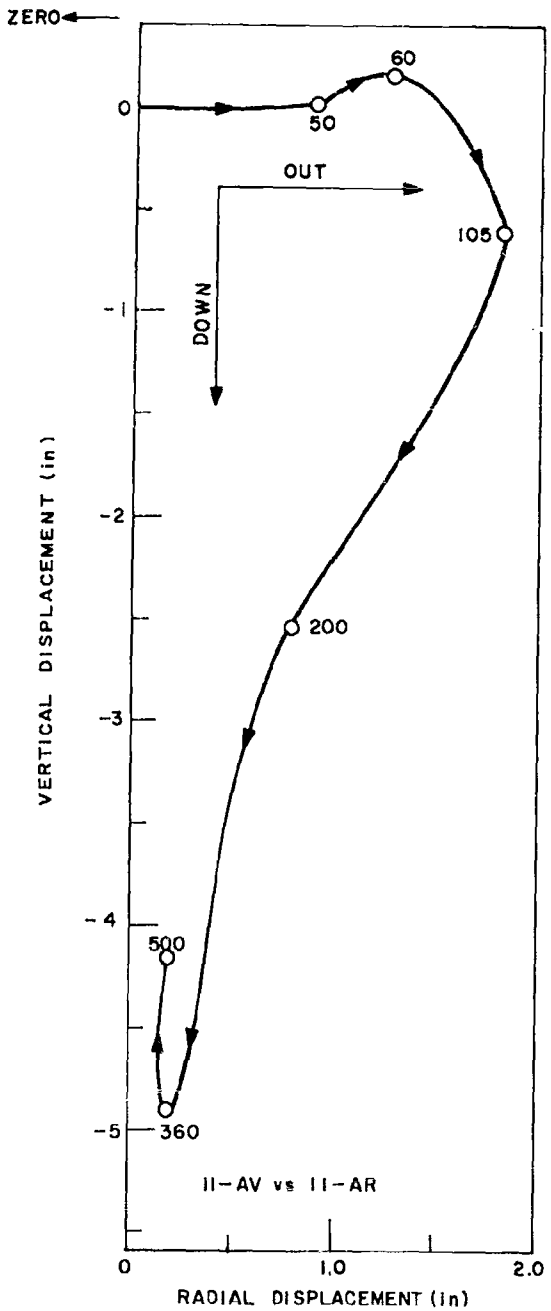

Figure 5.8 Displacement hodograph, Boring 11, vertical-radial.

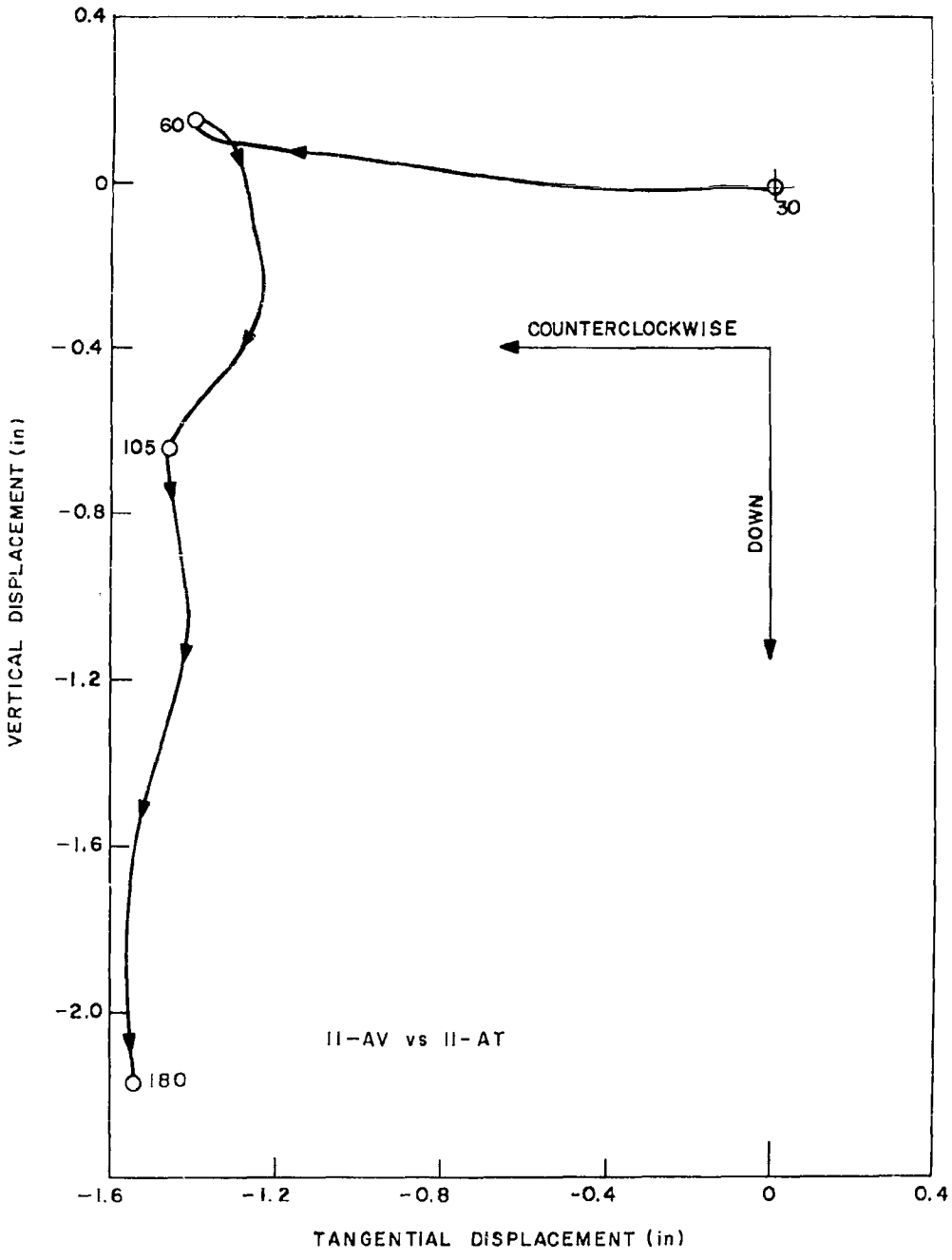

Figure 5.9 Displacement hodograph, Boring 11, vertical-tangential.

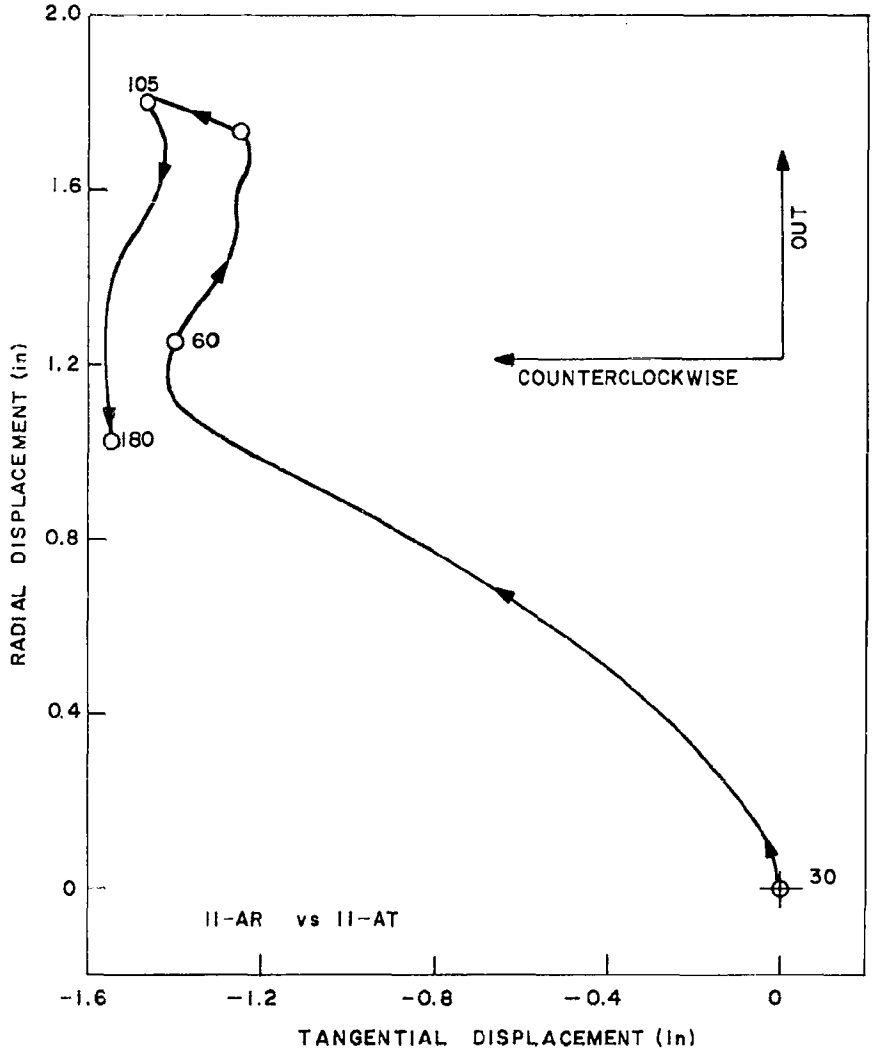

Figure 5.10 Displacement hodograph, Boring 11, radial-tangential.

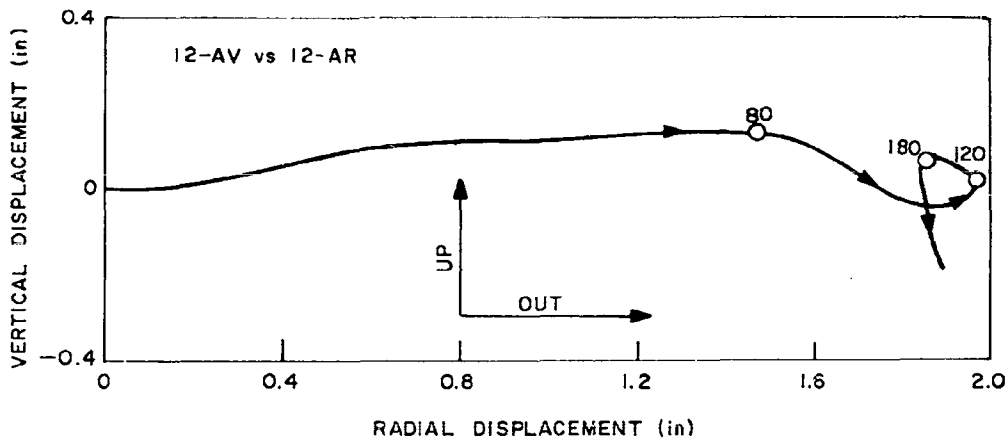

Figure 5.11 Displacement hodograph, Boring 12, vertical-radial.

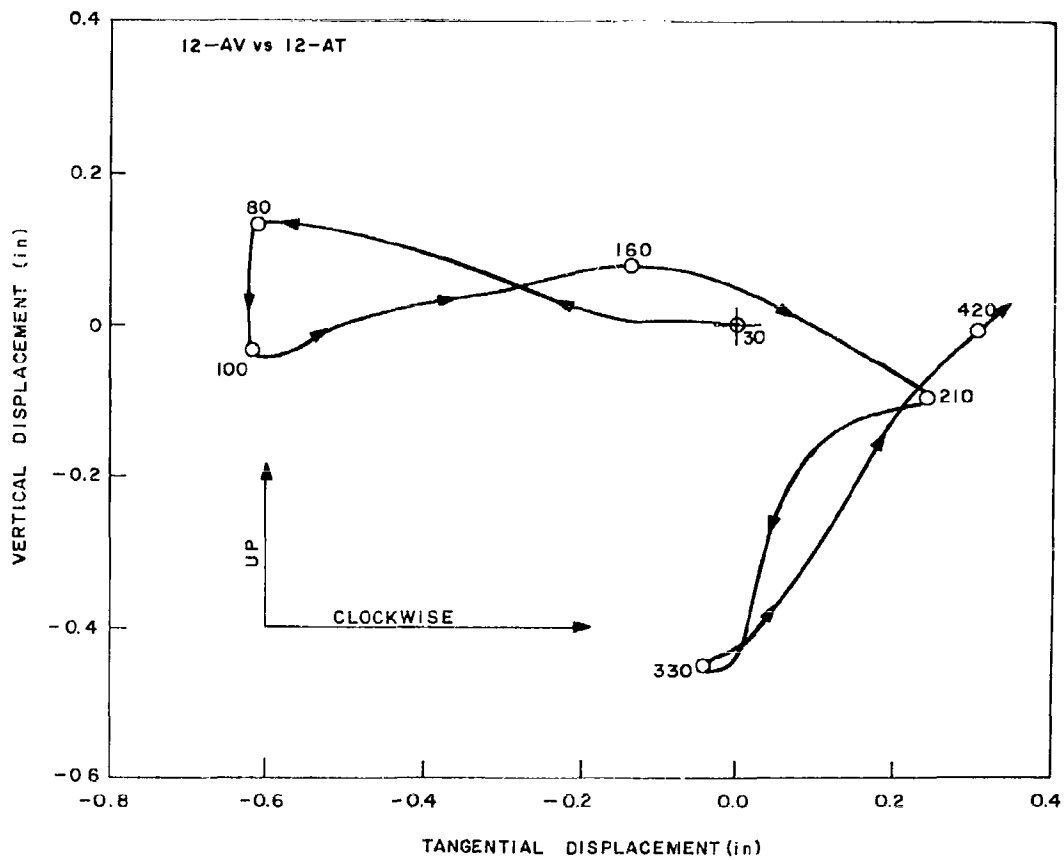

Figure 5.12 Displacement hodograph, Boring 12, vertical-tangential.

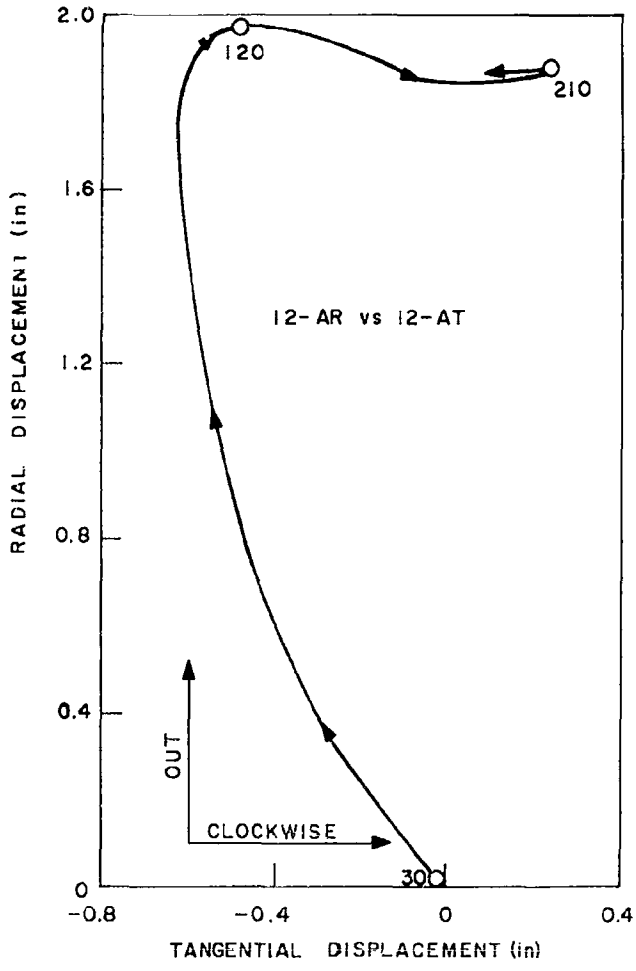

Figure 5.13 Displacement hodograph, Boring 12, radial-tangential.

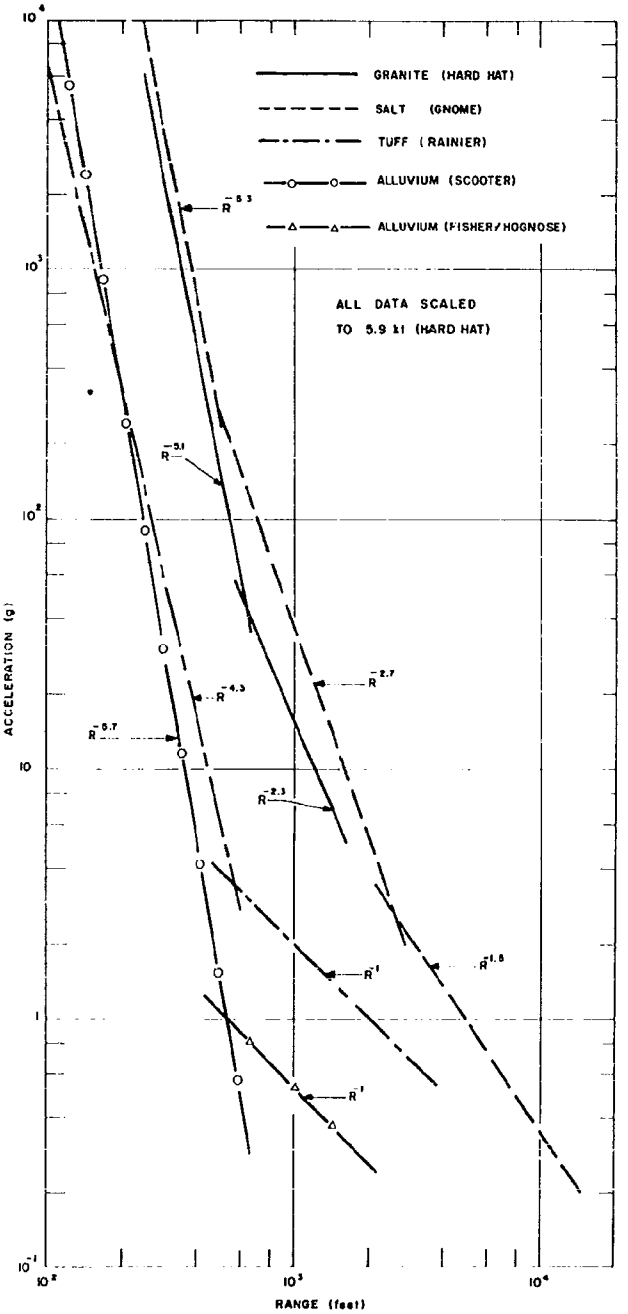

Figure 5.14 Acceleration versus range for granite, salt, tuff, and desert alluvium.

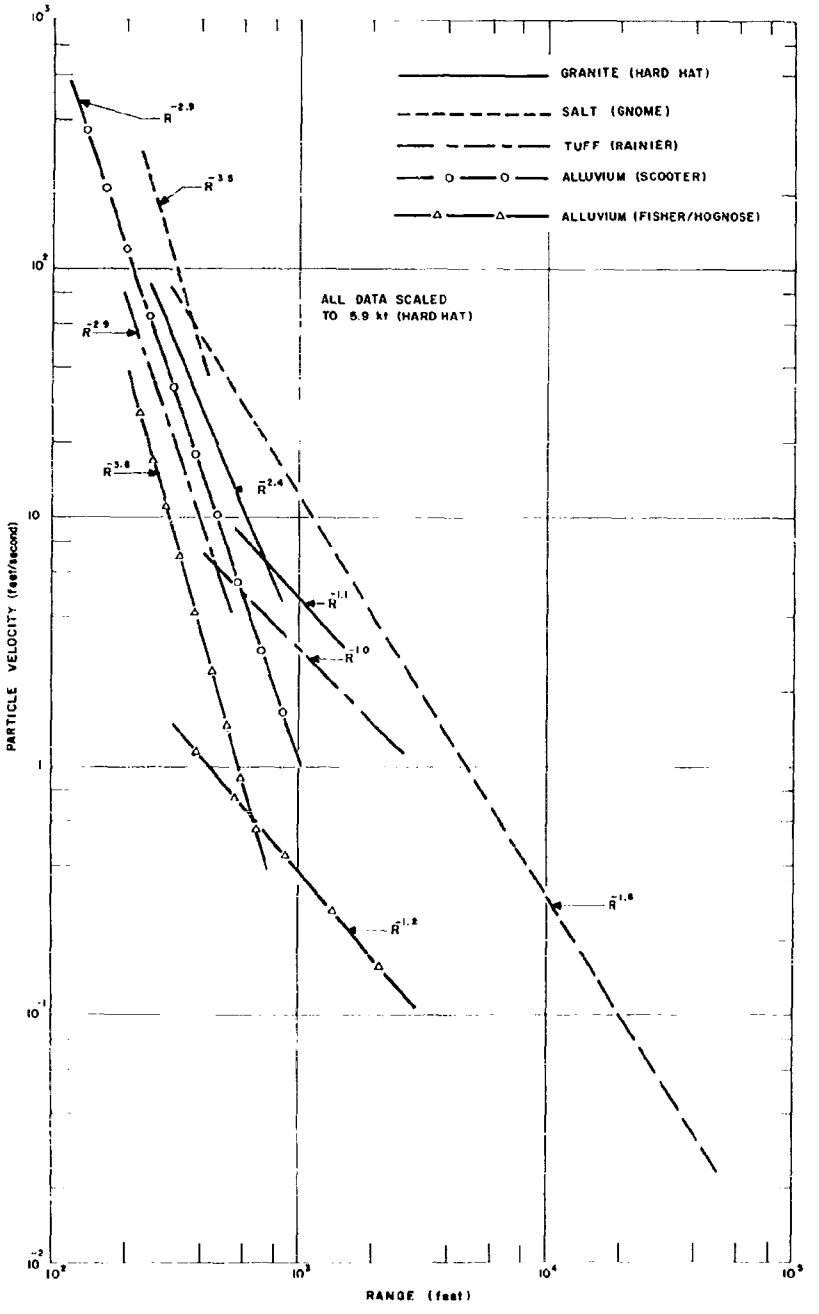

Figure 5.15 Particle velocity versus range for granite, salt, tuff, and desert alluvium.

Chapter 6

CONCLUSIONS AND RECOMMENDATIONS

6.1 CONCLUSIONS

Results obtained from Project 3.3 of the Hard Hat event give a good indication of how ground shock was transmitted through granitic rock between the hydrodynamic region and the elastic response domain. The description is not complete because of cable and instrument failures, but data are sufficient to establish the more pertinent features of rock response. From these considerations and analysis of the data, the following conclusions derive:

1. The ground shock propagated between the source and 784-foot radial range at a velocity of 18,128 feet per second, with a standard deviation of 177 feet per second, or less than 1 percent.
2. Project 3.3 instrumentation extended into the region of elastic or linear response only at the most remote station, 784 feet from the burst.
3. Radial acceleration maxima observed at five stations were outward and were attenuated as the inverse 5.12-power of radial range in the nonlinear region. Standard deviation

of the attenuation rate was about 5 percent, and average deviation of observed peak acceleration from the best curve was about 12.3 percent. The equation for the best-fit curve is

$$a = 9.89 \times 10^{15} R^{-5.12 \pm 0.26},$$

where acceleration, a, is in g-units, and range, R, in feet. Data from Project 1.2, at greater radial distance than Project 3.3 gages, helped define a region of reduced attenuation beyond 600 feet in which peak accelerations decrease as the inverse 2.92-power of range. Standard deviation of the attenuation rate is 9 percent, and average deviation of observed peak acceleration is 12.6 percent. The equation representing the best fit to data in this region is

$$a = 7.18 \times 10^{9} R^{-2.92 \pm 0.27}.$$

4. Radial component of particle velocity, u, in feet per second, both directly observed by velocity gages and derived by integration of acceleration data, included outward maxima and were attenuated as the inverse 2.41-power of range, R, in feet. Standard deviation of the attenuation rate was 9.4 percent. Average deviation of data, neglecting one obviously wild point, was 14 percent. The equation derived by least-squares fit to the data between 306- and 730-foot range is

$$u = 5.52 \times 10^{7} R^{-2.41 \pm 0.23}.$$

Again, data from Project 1.2 gages at 1500 feet helped define a region of lower attenuation rate beyond 730 feet, in which particle velocity decreased as the inverse 1.10-power of radial range. Standard deviation of the attenuation rate is 22 percent and average deviation of observed peak-particle velocities is 17.6 percent. The equation for best fit to these data is

$$u = 9.26 \times 10^{3} R^{-1.10 \pm 0.24}$$

5. Attenuation of particle velocity at a rate approximating the inverse first power of range implies transmission under conditions of linear or elastic response. The change in attenuation rate noted in Conclusion 4 indicates that linear response to Hard Hat shock must have begun near 730-foot range. Computation of elastic radius from estimated particle-velocity periods gives a value of 750 feet. Computed pressure at the transition to linear response is 4600 psi, a reasonable figure for the elastic limit of granite under transient loading.

6. Radial components of particle displacements derived by integration of acceleration and velocity data, and by direct measurement with displacement gages, includes much greater scatter than either acceleration or velocity maxima, and includes several points which are obviously

of negligible value. A least-squares fit to the data indicates that peak displacements are attenuated as the inverse 1.66-power of radial range with a standard deviation of about 23 percent of the attenuation rate. Average deviation of the observed data from the attenuation curve, ignoring three wild points, is about 38 percent. Attenuation of particle displacement, δ, in inches, is expressed by the equation

$$\delta = 1.17 \times 10^5 R^{-1.66 \pm 0.38},$$

where range, R, is in feet.

7. Residual displacements fall off from 90 percent of peak motion at 306 feet from the burst to 20 percent of peak at 604 feet, indicating a transition from highly nonlinear crushing toward linear elastic response of the rock beyond the more distant observation.
8. Transverse motion recorded at the two most remote Project 3.3 stations was notably one-sided, being initially outward, downward, and counterclockwise, as defined by displacements.
9. Radial stresses and strains are not sufficiently numerous or consistent to support analysis similar to particle motion. However, there is qualitative evidence that both stresses and strains are attenuated at a rate similar to that found for velocities. Stress-strain ratios of peaks are similar to the value of Young's modulus derived from granite cores

in the laboratory, with the exception of data from one station where high strain, low stress, and high particle velocity implies anomalously weak rock at the gage position.

10. Comparison of analyses of data from granite as characterized by Hard Hat results with similar analyses for bedded salt, tuff, and desert alluvium data indicates that peak accelerations in all four materials are attenuated at nearly the same rate, through the nonlinear response domain, but that accelerations in the hard rocks, granite and salt, are consistently two orders of magnitude higher than in the porous rocks within this region of response. This difference in magnitude is attributed to marked flattening of the shock-front rise in the porous materials before accelerations have been reduced to 10,000 g.

Particle velocity analyses are of more interest in their definition of onset of elastic response in the various media. For a 5.9-kt explosion, the elastic radius in tuff and alluvium is approximately 600 feet and in granite about 750 feet. Gnome data did not define a nonlinear-to-linear transition. Elastic limits of these rocks, as defined by computed pressures at the transition in particle velocity attenuation, are about 4600 psi in granite, 1450 psi in tuff, and 50 psi in desert alluvium.

A second group of conclusions relative to instrumentation performance follows:

1. Cable failures early in the recording period resulted in loss of portions of numerous records from both the radial instrumentation and the tunnel cross-section gages. In general, these cable failures appear to occur at or near the point of cable emergence into the tunnel, with the possible exception of the cables at Borings 4 and 6, which were probably crushed or sheared initially near the gage canister. Damage and loss of data from this project were appreciably less than from the similar measurement project for Gnome. Precautions taken in cable installation for Hard Hat as a result of the earlier Gnome experience, although not entirely effective, aided materially in producing data.
2. Gages performed well, with few exceptions. Accelerometers produced records without failure or major anomaly. Velocity gages performed reasonably well, but Hard Hat experience and, particularly, later field experience in Operations Nougat, have suggested that present methods of calibration are not wholly satisfactory. The inertial displacement gages and long-base strain gages used for Project 3.3 are not yet suitable for basic instrumentation, and further development

is necessary. In particular, the sensitivity of the inertial strain gage to tilt seriously limits its usefulness.

6.2 RECOMMENDATIONS

Results of Project 3.3 of Hard Hat have suggested certain needed developmental work and expansion of observational range for measurement of motion in rock near large explosions. Consequently, the following actions are recommended:

1. Observations should extend from the vicinity of the hydrodynamic region, as they did in Project 3.3, outward to include two or more stations within the region of linear response.
2. Accelerometers continue to be the most reliable particle-motion gage and should be primary instrumentation, although velocity gages appear to be very promising. The latter will develop greater reliability as more experience and improved methods of calibration are developed. Inertial displacement gages appear, in their present form, to be too sensitive to tilt to be satisfactory.
3. Further development work must be undertaken to provide reliable instruments for measuring stresses in the region from about 5 or 10 kilobars downward to 5 or 10 bars and to permit more effective installation of stress and strain gages in relatively deep borings.

4. Developmental work must continue to increase the effective life of information channels by hardening and protecting the signal cables.

5. Incorporation in the Shoal program of an expansion of the Hard Hat Project 3.3 instrument array, including a strategic distribution of backup instrumentation and the results of the developmental work recommended above, is highly desirable.

REFERENCES

1. F. N. Houser and F. G. Poole; "Granite Exploratio. Hole, Area 15, Nevada Test Site, Area 15; Part A. Structural, Petrographic, and Chemical Data"; TEM 836, U. S. Geological Survey, Washington, D. C.

2. Letter report, Symbol 14920, from Col. E. H. Lang, Waterways Experiment Station, Vicksburg, Mississippi, to Roger G. Preston, Lawrence Radiation Laboratory, Livermore, California, dated November 19, 1959.

3. L. M. Swift; "Development of an Earth Velocity Gage"; DASA-1191, October 31, 1960, Stanford Research Institute, Menlo Park, California.

4. W. R. Perret; "Ground Motion Studies at High Incident Overpressure"; Project 1.5, Operation Plumbbob, WT-1405, June 1960, Sandia Corporation, Albuquerque, New Mexico.

5. L. M. Swift; "Measurement of Close-in Earth Motion"; Project 1.2, Hard Hat Event, Nougat Series, VUP-2101, March 1962, Stanford Research Institute, Menlo Park, California;

6. Joseph A. Sharpe; "The Production of Elastic Waves by Explosion Pressures; I. Theory and Empirical Field Observations"; Geophysics, Volume 7, No. 2, April 1942.

7. H. R. Nicholls, Verne Hooker, and W. I. Duvall; "Dynamic Rock Mechanics Investigations, Project Cowboy"; Report APRL 38-3.2, September 1960; U. S. Bureau of Mines, Applied Physics Research Laboratories, College Park, Maryland.

8. V. R. McLamore and C. B. Forbes; "Compressional and Shear Wave Velocities"; Project 9.5, Hard Hat Event, Nougat Series, VUP-2500, April 1962;

9. W. D. Weart; "Particle Motion Near a Nuclear Detonation in Halite"; Project Gnome - Projects 44.1 and 1.1, PNE-108P, February 1962; Sandia Corporation, Albuquerque, New Mexico.

10. W. R. Perret; "Subsurface Motion from a Confined Underground Detonation - Part I"; Project 26.4b, Operation Plumbbob, WT-1529, August 1961, Sandia Corporation, Albuquerque, New Mexico.

11. W. R. Perret, A. J. Chabai, L. J. Vortman, and R. H. Bishop; "Mechanisms of Crater Formation"; Project Scooter, SC-4602(RR); Sandia Corporation, Albuquerque, New Mexico (to be published).

12. W. R. Perret; "Particle Motion Near Nuclear Detonations in Desert Alluvium"; Project 1.1, Fisher and Hognose Events, Nougat Series, VUP-2[illegible]; Sandia Corporation, Albuquerque, New Mexico (to be published).

DISTRIBUTION

Military Distribution Category 11

ARMY ACTIVITIES

1 CHIEF OF R & D DA
1 AC OF S INTELLIGENCE DA
1 CHIEF OF ENGINEERS DA
2 ARMY MATERIAL COMMAND
2 U S ARMY COMBAT DEVELOPMENTS COMMAND
1 DIRECTOR OF SPECIAL WEAPONS DEVELOPMENT OFFICE
1 U S ARMY ARTILLERY BOARD
1 U S ARMY AIR DEFENSE BOARD
1 U S ARMY COMMAND AND GENERAL STAFF COLLEGE
1 U S ARMY AIR DEFENSE SCHOOL
1 U S ARMY ARMORED SCHOOL
1 U S ARMY ARTILLERY & MISSILE SCHOOL
1 U S ARMY AVIATION SCHOOL
1 U S ARMY INFANTRY SCHOOL
1 U S ARMY ORDNANCE & GUIDED MISSILE SCHOOL
1 CHEMICAL CORPS TRAINING COMD
1 ENGINEER SCHOOL
1 ARMED FORCES INSTITUTE OF PATH
1 ARMY MEDICAL RESEARCH LAB
1 WALTER REED ARMY INST OF RES
1 ENGINEER RESEARCH & DEV LAB
1 WATERWAYS EXPERIMENT STATION
1 PICATINNY ARSENAL
1 DIAMOND ORDNANCE FUZE LABORATORY
2 BALLISTIC RESEARCH LABORATORY
1 WHITE SANDS MISSILE RANGE
1 U S ARMY MUNITIONS COMMAND
1 U S ARMY ELECTRONIC PROVING GROUND
1 U S ARMY COMBAT SURVEILLANCE AGENCY
1 THE RESEARCH & ANALYSIS CORP

NAVY ACTIVITIES

2 CHIEF OF NAVAL OPERATIONS OP03EG
1 CHIEF OF NAVAL OPERATIONS OP-75
2 CHIEF OF NAVAL RESEARCH
3 BUREAU OF NAVAL WEAPONS DLI-3
1 BUREAU OF SHIPS CODE 423
1 BUREAU OF YARDS & DOCKS
1 U S NAVAL RESEARCH LABORATORY
2 U S NAVAL ORDNANCE LABORATORY
1 NAVY ELECTRONICS LABORATORY
1 U S NAVAL MINE DEFENSE LAB
2 U S NAVAL RADIOLOGICAL DEFENSE LAB
2 U S NAVAL CIVIL ENGINEERING LAB
1 U S NAVAL SCHOOLS COMMAND TREASURE ISLAND
1 U S NAVAL POSTGRADUATE SCHOOL
1 U S NAVAL SCHOOL PORT HUENEME
1 NUCLEAR WEAPONS TRAINING CENTER ATLANTIC
1 NUCLEAR WEAPONS TRAINING CENTER PACIFIC
1 U S NAVAL DAMAGE CONTROL TNG CENTER
1 NAVAL AIR MATERIAL CENTER
1 U S NAVAL AIR DEVELOPMENT CENTER
1 US NAVAL AIR SP WPNS FACILITY
1 U S NAVAL MEDICAL RESEARCH INSTITUTE
1 DAVID W TAYLOR MODEL BASIN
1 U S NAVAL ENGINEERING EXPERIMENT STATION
1 NORFOLK NAVAL SHIPYARD
4 U S MARINE CORPS CODE A03H

AIR FORCE ACTIVITIES

1 HQ USAF AFTAC-TD
1 HQ USAF AFRDC-AE
1 HQ USAF AFRDR-MU
1 HQ USAF AFOCE
1 HQ USAF OPERATIONS ANALYSIS OFFICE
5 HQ USAF AFCIN-3D1
1 AC OF S INTELLIGENCE
1 DC OF S RESEARCH & TECHNOLOGY
1 THE SURGEON GENERAL
1 TACTICAL AIR COMMAND
1 AIR DEFENSE COMMAND
1 AIR FORCE SYSTEMS COMMAND
1 AIR FORCE BALLISTIC SYSTEMS DIVISION
1 RADC-RAALD,GRIFFISS AFB
1 PACIFIC AIR FORCES
1 SECOND AIR FORCE
2 AF CAMBRIDGE RESEARCH CENTER
5 AFSWC KIRTLAND AFB NMEX
2 AIR UNIVERSITY LIBRARY
1 LOWRY AFB
1 SCHOOL OF AVIATION MEDICINE
3 AERONAUTICAL SYSTEMS DIVISION
2 USAF PROJECT RAND
1 AIR TECHNICAL INTELLIGENCE CENTER
1 OFFICE OF AEROSPACE RESEARCH
1 HQ USAF AFORQ

OTHER DEPARTMENT OF DEFENSE ACTIVITIES

1 DIRECTOR OF DEFENSE RESEARCH AND ENGINEERING
1 ASST TO THE SECRETARY OF DEFENSE ATOMIC ENERGY
1 ADVANCE RESEARCH PROJECT AGENCY
1 WEAPONS SYSTEM EVALUATION GROUP
1 ASST SECRETARY OF DEFENSE INSTALLATION & LOGISTICS
4 DEFENSE ATOMIC SUPPORT AGENCY
1 FIELD COMMAND DASA
1 FIELD COMMAND DASA FCTG
2 FIELD COMMAND DASA FCWT
2 DEFENSE INTELLIGENCE AGENCY
1 ARMED SERVICES EXPLOSIVES SAFETY BOARD
1 JOINT TASK FORCE-8
1 COMMANDER-IN-CHIEF EUCOM
1 COMMANDER-IN-CHIEF PACIFIC
1 COMMANDER-IN-CHIEF ATLANTIC FLEET
1 STRATEGIC AIR COMMAND
1 CINCONAD
3 ASST SECRETARY OF DEFENSE CIVIL DEFENSE

ATOMIC ENERGY COMMISSION ACTIVITIES

3 AEC WASHINGTON TECH LIBRARY
2 LOS ALAMOS SCIENTIFIC LAB
5 SANDIA CORPORATION
10 LAWRENCE RADIATION LAB LIVERMORE
4 NEVADA OPERATIONS OFFICE,LAS VEGAS
1 DTIE OAK RIDGE,MASTER
30 DTIE OAK RIDGE SURPLUS